Study of a new low-oscillating second-order all-Mach number IMEX Finite Volume scheme for the full Euler equations

Paola Allegrini[1] Marie-Hélène Vignal[1]

Abstract

In this work, we propose and study an Implicit-Explicit (IMEX) finite volume scheme for the compressible Euler system which preserves the low Mach number limit. IMEX schemes are based on a flux splitting into a part treated explicitly and a part treated implicitly. We choose the flux splitting introduced by E. Toro and M.E. Vázquez-Cendón in [43] for ensuring the recognition of contact discontinuities and shear waves. Then, based on this flux splitting, we propose first and second order new linear asymptotic preserving (AP) schemes in the low Mach number limit. We prove that the schemes are asymptotically consistent, that is they degenerate into a consistent discretization of the incompressible system when the Mach number is sufficiently small. We perform a Fourier stability analysis on the linearized system around a constant state showing that the first order scheme is L^2 stable under a CFL condition independent of the Mach number. This proves the asymptotic stability in the linear case. We show one-dimensional and two-dimensional results which prove the good behavior of our scheme in all-Mach number regimes. Furthermore, following [18], we construct a low-diffusive TVD first-order scheme by interpolating the first-order in time scheme with a second-order one. Using MOOD process in one-dimensional numerical test-cases, we show that the MOOD process preserves the low oscillatory properties of the first-order scheme to the second-order scheme.

1 Introduction

Let $\Omega \subset \mathbb{R}^d$ ($d = 1$, 2 or 3) be an open bounded domain. The full Euler equations in rescaled variables are given by

$$\partial_t \rho(x,t) + \nabla \cdot \mathbf{q}(x,t) = 0, \tag{1a}$$

$$\partial_t \mathbf{q}(x,t) + \nabla \cdot \big(\rho(x,t)\mathbf{u}(x,t) \otimes \mathbf{u}(x,t)\big) + \frac{1}{\varepsilon}\nabla p(x,t) = 0, \tag{1b}$$

$$\partial_t E(x,t) + \nabla \cdot \big((E(x,t) + p(x,t))\,\mathbf{u}(x,t)\big) = 0, \tag{1c}$$

where $x \in \Omega$ and $t \in \mathbb{R}^+$ are the space and time variables, the unknown and flux vectors are $W = (\rho, \mathbf{q}, E)$ and $F(W) = (\mathbf{q}\,,\, \rho\mathbf{u} \otimes \mathbf{u} + 1/\varepsilon\, p\, \mathrm{Id}_{\mathbb{R}^3}\,,\, (E+p)\,\mathbf{u})$ with $\rho > 0$ the density of the fluid, $\mathbf{q} = \rho\,\mathbf{u}$ its momentum, $\mathbf{u}$ its velocity, E its total energy and $p > 0$ its pressure given by an equation of state, here that of perfect gases with $\gamma > 1$ the ratio of specific heats:

$$E = \frac{p}{\gamma - 1} + \frac{\varepsilon}{2}\frac{|\mathbf{q}|^2}{\rho}. \tag{1d}$$

The rescaled parameter ε is related to the Mach number $M^2 = u_0^2/c_0^2 = \varepsilon/\gamma$, with $c_0^2 = \gamma\ p_0/\rho_0$, u_0, p_0 and ρ_0 being the reference values of the velocity norm, pressure and density in the fluid. In low Mach number regimes, the reference sound speed in the fluid, c_0, is very large compared to the reference speed of the fluid itself, u_0, and so ε is very small. It is well known that in such situations

[1]Institut de Mathématiques de Toulouse (IMT); UMR5219, Université de Toulouse ; CNRS, UPS, F-31062 Toulouse Cedex 9, France Paola.Allegrini@math.univ-toulouse.fr, mhvignal@math.univ-toulouse.fr.
This work was funded by the French ANR project MUFFIN, contract number: ANR-19-CE46-0004.

(see [42]), if an explicit scheme is used, the time step must satisfy a severe CFL (Courant-Friedrichs-Levy) stability condition. Indeed, for $d = 1$, the eigenvalues of the Jacobian matrix, $DF(W)$, are given by $\lambda_1 = \mathbf{u} - c/\sqrt{\varepsilon}$, $\lambda_2 = \mathbf{u}$ and $\lambda_3 = \mathbf{u} + c/\sqrt{\varepsilon}$ with $c^2 = \gamma\, p/\rho$ and the CFL condition, ensuring the stability of explicit schemes, for the time and space steps Δt and Δx, is given by $\Delta t \leq \Delta x/\max(|\mathbf{u} \pm c/\sqrt{\varepsilon}|)$. Then, for a given space step Δx, the time step Δt is of order $\sqrt{\varepsilon}$ and tends to 0 with ε. Furthermore, even if this constraint is satisfied, it is also well known (see [27], [26] or [17]) that explicit schemes with classical solvers suffer from a consistency problem in the limit $\varepsilon \to 0$. They are not capable to capture the right asymptotic regime. A solution is proposed in [17] consisting in modifying the solver to well captured the asymptotic limit, but, the stability constraint on the time step still remains.

A possible way to bypass these limitations is to use the incompressible Euler equations obtained as the low Mach number limit of the compressible Euler equations (1). The rigorous low Mach number limit of the compressible Euler system has been widely studied in the last years [30, 31, 40, 2, 32]. Results in the case of the non-isentropic Euler equations with general initial data can be found in [34] in the free space $\Omega = \mathbb{R}^d$, in [1] for an exterior domain and in a bounded toroidal domain in [35]. Here, we briefly recall the formal limit.

We denote by $(\rho^{(\varepsilon)}, \mathbf{q}^{(\varepsilon)}, E^{(\varepsilon)}, p^{(\varepsilon)})$ the solution of (1) with the impermeability boundary condition $\mathbf{u}^{(\varepsilon)} \cdot \nu = 0$ on $\partial\Omega$ where ν is the unit normal to $\partial\Omega$ outward to Ω. Note that no assumptions are made on the initial conditions.
Classically, we write the expansions of the variables $f^{(\varepsilon)} = \rho^{(\varepsilon)}$, $\mathbf{u}^{(\varepsilon)}$, $p^{(\varepsilon)}$, $E^{(\varepsilon)}$ in powers of the Mach number $\sqrt{\varepsilon}$: $f^{(\varepsilon)} = f^{(0)} + \sqrt{\varepsilon}\, f^{(1)} + \varepsilon\, f^{(2)} + \cdots$
We insert this expansion into the Euler system (1), we obtain

$$\nabla p^{(0)} = \nabla p^{(1)} = 0, \tag{2a}$$
$$\partial_t \rho^{(0)} + \nabla \cdot \mathbf{q}^{(0)} = 0, \tag{2b}$$
$$\partial_t \mathbf{q}^{(0)} + \nabla \cdot \big(\rho^{(0)}\, \mathbf{u}^{(0)} \otimes \mathbf{u}^{(0)}\big) + \nabla p^{(2)} = 0, \tag{2c}$$
$$\partial_t E^{(0)} + \nabla \cdot \big((E^{(0)} + p^{(0)})\, \mathbf{u}^{(0)}\big) = 0, \tag{2d}$$
$$E^{(0)} = \frac{p^{(0)}}{\gamma - 1}. \tag{2e}$$

Now (2a) yields $p^{(0)}(x,t) = p^{(0)}(t)$ for all $x \in \Omega$ and $t > 0$. Note that the initial pressure does not necessarily satisfy this property. Using (2e), we obtain $E^{(0)}(x,t) = E^{(0)}(t) = p^{(0)}(t)/(\gamma - 1)$ for all $x \in \Omega$ and $t > 0$ and so (2d) integrated on $\Omega \times [0,t]$ gives

$$|\Omega| E^{(0)}(t) = \int_\Omega E^0(x,0)\, dx - \int_0^t (E^{(0)}(s) + p^{(0)}(s)) \int_\Omega \nabla \cdot \mathbf{u}^{(0)}(x,s)\, dx\, ds = \int_\Omega E^0(x,0)\, dx,$$

thanks to the impermeability boundary condition $\mathbf{u}^{(0)} \cdot \nu = 0$ on $\partial\Omega$.
By considering again the leading order energy equation (2d), we recover the incompressibility condition $\nabla \cdot \mathbf{u}^0 = 0$ and the incompressible limit system [1]:

$$\partial_t \rho^{(0)} + \mathbf{u}^{(0)} \cdot \nabla \cdot \rho^{(0)} = 0, \tag{3a}$$
$$\partial_t \mathbf{q}^{(0)} + \nabla \cdot \big(\rho^{(0)}\, \mathbf{u}^{(0)} \otimes \mathbf{u}^{(0)}\big) + \nabla p^{(2)} = 0, \tag{3b}$$
$$\nabla \cdot \mathbf{u}^{(0)} = 0, \tag{3c}$$
$$E^{(0)} = \frac{p^{(0)}}{\gamma - 1} = \frac{1}{|\Omega|} \int_\Omega E^{(0)}(x,0)\, dx. \tag{3d}$$

Remark 1 *Note that the same results can be obtained on $p^{(1)}$, $E^{(1)}$ and $\mathbf{u}^{(1)}$. Indeed, writing the following orders of the energy and state equations, we have $\partial_t E^{(1)} + \nabla(E^{(1)} + p^{(1)}) \cdot \mathbf{u}^{(0)} + (E^{(0)} + p^{(0)}) \nabla \cdot \mathbf{u}^{(1)} = 0$, and $E^{(1)} = p^{(1)}/(\gamma - 1)$. We recall that thanks to* (2a), *$\nabla p^{(1)} = 0$, and so $\nabla E^{(1)} = 0$. Now, integrating the first order energy equation on $\Omega \times [0, t]$ and using the impermeability conditions $\mathbf{u}^{(1)} \cdot \nu = 0$ on $\partial\Omega$, we recover $E^{(1)} = p^{(1)}/(\gamma - 1) = \frac{1}{|\Omega|} \int_\Omega E^{(1)}(x, 0)\, dx$. Therefore, using the initial conditions we can determine $p^{(0)}$ and $p^{(1)}$ which are constant. Note that we also have $\nabla \cdot \mathbf{u}^{(1)} = 0$ but $\mathbf{u}^{(1)}$ cannot be determined without $p^{(3)}$. Note also that the total energy can be determined up to the second-order correction, since the second-order term in the equation of state gives $E^{(2)} = p^{(2)}/(\gamma - 1) + \rho^{(0)} |\mathbf{u}^{(0)}|^2/2$.*

Following this formal analysis, like in [17], the initial conditions of the Euler system (1), are said well-prepared for the incompressible regime if

$$p(x, 0) = p^\star + \varepsilon\, \overline{p}(x), \qquad \text{and } \mathbf{u}(x, 0) = \mathbf{u}^\star(x) + \sqrt{\varepsilon}\, \overline{\mathbf{u}}(x), \tag{4}$$

with $p^\star$ a positive constant and $\nabla \cdot \mathbf{u}^\star = 0$.

An explicit equation for the second-order pressure correction $p^{(2)}$ can be obtained using the velocity equation: $\rho^{(0)}\, \partial_t \mathbf{u}^{(0)} + \rho^{(0)}\, (\mathbf{u}^{(0)} \cdot \nabla)\mathbf{u}^{(0)} + \nabla p^{(2)} = 0$. Dividing this equation by $\rho^{(0)}$, taking the divergence and using the compressibility constraint $\nabla \cdot \mathbf{u}^{(0)} = 0$, we obtain an elliptic equation for $p^{(2)}$:

$$-\nabla \cdot \left(\frac{1}{\rho^{(0)}} \nabla p^{(2)} \right) = \nabla \cdot \Big((\mathbf{u}^{(0)} \cdot \nabla)\mathbf{u}^{(0)} \Big). \tag{5}$$

The resulting system, changing (3c) into (5) is called the reformulated incompressible Euler system. This limit model does no longer depend on ε and so is no longer constrained by the small values of ε. But, it can be used only in the regions where the fluid is incompressible and so in the regions in space and time where ε is sufficiently small. In the regions where ε takes on order one or intermediate values, the compressible Euler equations (1) must be used. Then, two models must be used which leads to other difficulties like the detection of the interface between the two models, the reconnection at the interface...

Another possible solution consists in using only one model, the compressible Euler equations (1), valid everywhere and at every time. However, an asymptotic preserving scheme, free of the constraints related to the Mach number ε, must be used. Such schemes have been developed in literature, see [16, 14, 15, 28, 41, 24, 6, 19, 7, 18, 33] for the isentropic Euler system and [37, 13, 38, 23, 11, 19, 7, 18, 8] for the full Euler system. They permit to use time steps bounded in the limit ε tends to 0, the schemes are said to be asymptotically stable. Their consistency error does not increase when the Mach number tends to 0, so they lead to consistent approximations of the limit incompressible model when the low Mach number goes to zero. This corresponds to the asymptotic consistency property. A scheme satisfying both asymptotic stability and asymptotic consistency is said asymptotic preserving.

In practice, one way for obtaining asymptotic preserving finite volume schemes is to use IMEX methods ([3],[39]). In our case, the flux of the Euler system (1) is split into two parts $F = F_e + F_i$. The first one, F_e, will be treated explicitly while the other one, F_i, will be treated implicitly. This flux splitting must be well chosen in order to obtain both asymptotic stability and asymptotic consistency and such that the cost of the resolution of the scheme is not too high especially when ε is of order 1 in compressible regimes. It is also important to conserve some of the properties of

the classical explicit schemes like the cost of an iteration in time and the preservation of stationary states.

In the isentropic case, the choice of the flux splitting to construct asymptotic preserving schemes in the low Mach number limit, is well identified and widely used in the literature [24, 6, 19, 7, 18, 33]. For the full Euler equations case, we can find different flux splittings in the literature leading to different asymptotic preserving schemes, see [13, 23, 11, 19, 7, 4, 8]. Here, based on the analysis of the asymptotic preserving properties (stability and consistency), we select the flux splitting introduced in [43] for constructing a linear IMEX AP scheme. We propose a new linear asymptotic preserving scheme based on the non-linear semi-discretization proposed in [8]. We prove the asymptotic consistency as well as its preservation of constant contact discontinuities.

Furthermore, we numerically show that an upwinding on the implicit numerical fluxes is necessary to reduce some non-physical oscillations. Then, using a Fourier linear stability analysis we prove that this new AP scheme is linearly L^2 stable under a CFL condition independent of the Mach number ε. Numerical simulations presented in Section 3.4 show the good behavior of the first-order scheme in all regimes. Like in [18] for the isentropic case, in Section 4 we propose and study a second-order extension based on the ARS-IMEX scheme ([3]). We prove its asymptotic consistecy and show several one-dimensional and two-dimensional numerical results.
Furthermore, we propose a MOOD process (see [21], [22]) in order to preserve the low oscillatory properties of the first-order scheme to the second-order schemes. The MOOD procedure consists of using at each time step the oscillating second-order scheme when no oscillations appear. If oscillations are detected, the second-order scheme is replaced by a low-oscillating first-order AP scheme. The main difficulties of the MOOD procedure are the detection of the oscillations and the choice of a low-oscillating first-order AP scheme as less diffusive as possible. Here, we first construct a low-oscillating and low-diffusive first-order AP scheme called TVD-AP scheme and we propose an original detection criterion which allows in one-dimensional numerical simulations to significantly reduce the oscillations of the second-order scheme while guaranteeing an accuracy close to that of the second-order scheme.

2 Analysis of the flux splitting

There exist several splittings for the full Euler system in the literature, all leading to different IMEX asymptotic preserving (AP) schemes. In this section, we first discuss the properties that are essential for building an efficient AP scheme in the low Mach number limit. These properties naturally lead us to choose a splitting initially introduced by E. Toro and M.E. Vázquez-Cendón in [43] but not in the context of AP schemes. We show that this splitting satisfies all the properties listed above. Then, we present and study several splittings close to the one we have chosen. It is important to note that this splitting of Toro and Vázquez-Cendón yields non-linear schemes, see [23] or [8]. Then, in the next section, we show how this non-linear splitting can be linearized, thus leading to a new linear AP scheme.

2.1 Choice of the flux splitting

In order to build an IMEX finite volume AP scheme in the low Mach number regimes, we must decide which terms should be treated implicitly and so we must set a flux decomposition $F = F_i + F_e$. If a first-order scheme is considered, the parts F_e and F_i will be respectively explicitly

and implicitly discretized leading to the following semi-discretization

$$\frac{W^{n+1}-W^n}{\Delta t}+\nabla\cdot F_e(W^n)+\nabla\cdot F_i(W^{n+1})=0. \tag{6}$$

Let us first note that a fully implicit scheme ($F_e=0$, $F_i=F$) is of course asymptotic preserving but its implementation requires the resolution of a complex non-linear system, which can be very costly. Moreover, the introduction of implicit terms increases the viscosity of the scheme and thus decreases its accuracy. Finally an implicit treatment of the whole flux is not necessary to build an AP scheme. We therefore wish to treat implicitly as few terms as possible while guaranteeing the AP character of the scheme.

Furthermore, for an explicit collocated scheme, $F_e=F$ and $F_i=0$. In this case, we have seen that the scheme is not asymptotically stable since the CFL decreases with ε. In addition, without corrections of the numerical fluxes, see [26] or [17], the scheme is not asymptotically consistent either. In particular, the formal limit ε tends to 0 of the explicit semi-discretization in time gives only the constraint $\nabla p^n=0$ on W^n when W^{n+1} is calculated. An implicit discretization of the pressure gradient term in the momentum equation is necessary to obtain the asymptotic consistency. But, this is not sufficient since we must recover $\nabla\cdot\mathbf{u}^{n+1}=0$ from the energy equation like in the continuous case. This means that a part of the energy flux term $(E+p)\,\mathbf{u}$ must be treated implicitly.

To better understand how to choose the implicit part of the energy flux, we first reformulate the compressible Euler model as done for the incompressible model to obtain equation (5). We begin from (1) with the velocity equation obtained from the momentum and mass conservation:

$$\rho\,\partial_t\mathbf{u}+\rho\,(\mathbf{u}\cdot\nabla)\,\mathbf{u}+\frac{1}{\varepsilon}\,\nabla p=0.$$

In the case of the incompressible system, we used the incompressibility constraint $\nabla\cdot\mathbf{u}=0$ which comes from the limit of the energy equation and is no longer true in the compressible regime. But, we can still use the energy equation, which, using the mass and momentum equations for eliminating the kinetic part, can be rewritten:

$$\partial_t E+\nabla\cdot((E+p)\,\mathbf{u})=\partial_t k_\varepsilon+\partial_t\frac{p}{\gamma-1}+\nabla\cdot((k_\varepsilon+h)\,\mathbf{u})=\partial_t\frac{p}{\gamma-1}+\frac{\mathbf{u}\cdot\nabla p}{\gamma-1}+\frac{\gamma p}{\gamma-1}\,\nabla\cdot\mathbf{u}=0, \tag{7}$$

where $k_\varepsilon=\varepsilon\,\rho\,|\mathbf{u}|^2/2$ is the kinetic energy and $h=\gamma p/(\gamma-1)$ is the enthalpy. Now, dividing the velocity equation by ρ and the internal energy equation (7) by the enthalpy, taking the divergence of the first resulting equation and the time derivative of the second one and subtracting the results, we obtain the following equation

$$\partial_t\left(\frac{\partial_t p}{\gamma\,p}+\frac{\mathbf{u}\cdot\nabla p}{\gamma\,p}\right)-\frac{1}{\varepsilon}\nabla\cdot\left(\frac{1}{\rho}\,\nabla p\right)=\nabla\cdot\Big((\mathbf{u}.\nabla)\,\mathbf{u}\Big),$$

which is the non-linear pressure wave equation in the fluid.

From a numerical point of view, if the second-order derivative term in space $\nabla\cdot(1/\rho\,\nabla p)$, in this pressure wave equation is explicit, we must impose Δt of the order of $\sqrt{\varepsilon}\,\Delta x$ for ensuring the stability of the scheme. We recover the classical non uniform CFL constraint.

Then, for constructing a scheme for the Euler system (1), asymptotically stable (i.e. with a CFL uniform with respect to ε), the time discretization must lead to an implicit discretization of this second-order derivative term in space and thus, we need an implicit discretization of the term

$\gamma p/(\gamma-1)\,\nabla\cdot\mathbf{u}$ in Eq. (7). Since we must work with the conservative variables, we need an implicit discretization of the term $\nabla\cdot(h\,\mathbf{u})$ in the energy flux in the Euler equations. A possible choice for the flux splitting is then given by

$$F_e(W)=\Big(\mathbf{q},\,\rho\mathbf{u}\otimes\mathbf{u},\,k_\varepsilon(W)\,\mathbf{u}\Big),\qquad F_i(W)=\left(0,\frac{1}{\varepsilon}\,p\,\mathrm{Id}_{\mathbb{R}^3}\,,\,h(W)\,\mathbf{u}\right),\tag{8}$$

where $k_\varepsilon(W)=\varepsilon\,\rho\,|\mathbf{u}|^2/2$ and $h(W)=\gamma p/(\gamma-1)=\gamma\,(E-k_\varepsilon(W))$.

Note that this flux splitting was first introduced in [43] but not in the context of AP schemes in the low Mach number limit. The authors consider this flux splitting for building schemes which ensure the recognition of contact discontinuities and shear waves. This splitting has been also used in [23], [8], [9] for constructing IMEX AP schemes in low Mach number regimes leading to non-linear schemes.

Let us study the asymptotic properties of this splitting. In the case of the isentropic Euler system, it has been shown in [19] with a one-dimensional linear stability analysis, that the CFL stability condition of such IMEX schemes is only related to the eigenvalues of the explicit matrix DF_e. Furthermore, the upwinding of the explicit numerical fluxes must be related only to the eigenvalues of the explicit matrix DF_e, the Jacobian matrix of the explicit part of the flux. The implicit part of the flux, F_i can be discretized with a centered solver. In this case the scheme will be only L^2 stable and some oscillations may appear during the simulations but they are damped for long times. These oscillations can be removed, or at least reduced, using an upwind solver for the implicit part. This upwinding can depend on the eigenvalues of the implicit matrix DF_i (the Jacobian matrix of the part of the flux which is implicitly discretized) but the stability condition will not be modified. Following this result, for ensuring the asymptotic stability of the scheme, it is necessary that each of the Jacobian matrices (DF_e and DF_i) have real eigenvalues, and those of DF_e must be uniformly bounded with respect to ε.
Furthermore, the asymptotic consistency consists in recovering an approximation of the incompressible Euler equations (3) when ε tends to zero. Finally, a fluid with constant velocity and pressure is a stationary solution of the incompressible Euler equations and a constant contact discontinuity of the compressible Euler system. We show that the scheme preserves these stationary incompressible solutions and constant contact discontinuities.

We prove the following result

Lemma 1 *Assuming impermeability boundary conditions ($\mathbf{u}\cdot\nu=0$ on $\partial\Omega$), the semi-discretization* (6), (8) *satisfies the following properties:*

(i)- Necessary condition for the asymptotic stability: In one dimension, each of the Jacobian matrices DF_e and DF_i have real eigenvalues. Those of DF_e are uniformly bounded.

(ii)- Asymptotic consistency: In the limit $\varepsilon\to 0$, from the semi-discretization in time, we formally recover an approximation of the incompressible Euler equations (3). *In particular, we have*

$$E^{n+1}=\frac{p^{n+1}}{\gamma-1}=\frac{1}{|\Omega|}\int_\Omega E^0(x)\,dx,$$

and so $\nabla p^{n+1}=\nabla E^{n+1}=0$ for all $n\geq 0$ and, $\nabla\cdot\mathbf{u}^{n+1}=0$ for all $n\geq 1$.

(iii)- Preservation of constant contact discontinuities: if $D\mathbf{u}^n(x)=0$ and $\nabla p^n(x)=0$, then there exists a solution W^{n+1} such that $D\mathbf{u}^{n+1}(x)=0$ and $\nabla p^{n+1}(x)=0$, where $D\mathbf{u}(x)=(\partial_{x_j}\mathbf{u}_i(x))_{1\leq i,j\leq d}$ denotes the Jacobian matrix of $\mathbf{u}=(u_1,\cdots,u_d)\in\mathbb{R}^d$.

proof Concerning assertion (i). In one dimension, a simple calculation shows that the eigenvalues of DF_e are given by 0 and $\mathbf{u}$ of multiplicity 2 while those of DF_i are given by 0 and $\mathbf{u}/2 \pm \sqrt{\mathbf{u}^2/4 + c^2/\varepsilon}$ where we recall that $c^2 = \gamma\, p/\rho$.

It has been already proven in [8] that this splitting satisfies (ii) with initial conditions which are not necessary well-prepared for the incompressible limit (that is initial conditions with a pressure and a velocity respectively close to a constant and a divergence-free vector field, see (4)).

Let us now prove (iii). If $\mathbf{u}^n(x) = \overline{\mathbf{u}} \in \mathbb{R}^d$ and $p^n(x) = \overline{p} > 0$ are constant, the mass equation gives $\rho^{n+1} = \rho^n - \Delta t\, \overline{\mathbf{u}} \cdot \nabla \rho^n$. Then, thanks to the momentum equation

$$\rho^{n+1}\, \mathbf{u}^{n+1} = (\rho^n - \Delta t\, \overline{\mathbf{u}} \cdot \nabla \rho^n)\, \overline{\mathbf{u}} - \frac{\Delta t}{\varepsilon} \nabla p^{n+1} = \rho^{n+1}\, \overline{\mathbf{u}} - \frac{\Delta t}{\varepsilon} \nabla p^{n+1}.$$

So, there exists a solution such that $\mathbf{u}^{n+1} = \overline{\mathbf{u}}$ and $p^{n+1} = \overline{p}$, since the previous equation yields $\rho^{n+1}\, \overline{\mathbf{u}} = \rho^{n+1}\, \overline{\mathbf{u}}$ and the energy equation yields

$$E^{n+1} = \frac{\overline{p}}{\gamma - 1} + \varepsilon\, \rho^{n+1}\, \frac{\overline{\mathbf{u}}^2}{2} = E^n - \Delta t\, \overline{\mathbf{u}} \cdot \nabla k^n = \frac{\overline{p}}{\gamma - 1} + \varepsilon\, \rho^n\, \frac{|\overline{\mathbf{u}}|^2}{2} - \Delta t\, \overline{\mathbf{u}} \cdot \nabla \left(\varepsilon \rho^n\, \frac{|\overline{\mathbf{u}}|^2}{2} \right)$$

and so we recover the mass transport equation $\rho^{n+1} = \rho^n - \Delta t\, \overline{\mathbf{u}} \cdot \nabla \rho^n$.

Remark 2 *1. We will see in the linear Fourier stability analysis and in the numerical simulations that it seems not necessary to have the hyperbolicity of each "sub-matrix", DF_e and DF_i, they could have multiple real eigenvalues and not be diagonalizable.*

2. Note that the implicit treatment of the full "enthalpy term" in the energy equation is necessary for the asymptotic consistency: if we change the flux splitting to become

$$F_e(W) = (\mathbf{q},\, \rho \mathbf{u} \otimes \mathbf{u},\, k_\varepsilon(W)\, \mathbf{u} + \beta\, h(W)\, \mathbf{u}) \text{ and } F_i(W) = \left(0, \frac{1}{\varepsilon}\, p\, Id_{\mathbb{R}^3},\, (1 - \beta)\, h(W)\, \mathbf{u} \right),$$

with $\beta \in [0, 1[$, then Property (ii) is lost. Indeed, like for $\beta = 0$, the limit $\varepsilon \to 0$ gives $\nabla p^{n+1} = \nabla E^{n+1} = 0$ for all $n \geq 0$, but now for all $n \geq 1$,

$$\nabla \cdot \mathbf{u}^{n+1} = \frac{\beta}{\beta - 1}\, \nabla \cdot \mathbf{u}^n.$$

The incompressibility constraint is recovered only if $\beta = 0$ or if the initial velocity, used for (6), is well-prepared for the incompressible limit i.e. if the initial velocity is close to a divergence-free velocity such that $\mathbf{u}^0(x) = \mathbf{u}^\star(x) + \sqrt{\varepsilon}\, \overline{\mathbf{u}}(x)$ with $\nabla \cdot \mathbf{u}^\star = 0$, see (4). So the energy flux splitting corresponding to $\beta = 0$ is the only choice which ensures the asymptotic consistency.

2.2 Properties of some other all-Mach number IMEX finite volumes schemes

Let us look at the properties $(i) - (iii)$ of Lemma 1 for some flux splittings found in the literature. It is not possible to be exhaustive, as there is far too much works on the subject, so we limit ourselves to flux splittings close to the one considered in this article.

In the pioneering work [13], the authors proposed the following flux splitting: in (6), $F_e(W^n) + F_i(W^{n+1})$ is replaced by $F^{n,n+1}$ where

$$F^{n,n+1} = \left(\mathbf{q}^n,\, \rho^n \mathbf{u}^n \otimes \mathbf{u}^n + \alpha\, p^n \mathrm{Id}_{\mathbb{R}^3} + \left(\frac{1}{\varepsilon} - \alpha \right) p^{n+1}\, \mathrm{Id}_{\mathbb{R}^3}\,,\, \frac{E^n + p^n}{\rho^n}\, \mathbf{q}^{n+1} \right), \tag{9}$$

with $E^{n+1} = p^{n+1}/(\gamma - 1) + \varepsilon\, \rho^n\, |\mathbf{u}^n|^2/2$, and where $\alpha \geq 0$ must be well chosen for insuring the asymptotic stability and avoid oscillations. In many test-cases, in particular when ε is small, the authors choose $\alpha = 0$ but $\alpha = 10$ is also considered when ε is of order 1 to prevent spurious oscillations. The previous semi-discretization, cannot be written in a conservative flux splitting form $F_e(W^n) + F_i(W^{n+1})$. Even for $\alpha = 0$ it is a multi-step-method since $p^n = (\gamma - 1)(E^n - \varepsilon\, \rho^{n-1}\, |\mathbf{u}^{n-1}|^2/2)$ (except perhaps for p^0) and so depends on E^n and $(\rho^{n-1}, \mathbf{q}^{n-1})$ so the energy flux $(E^n + p^n)\, \mathbf{q}^{n+1}/\rho^n$ depends on W^{n+1}, W^n and W^{n-1}. The scheme cannot be written (in one dimension) in the following non conservative form $A_e\, \partial_x W^n + A_i\, \partial_x W^{n+1}$. Then, (i) is meaningless and the semi-discretization is outside the scope of our study. Note that Properties (ii) and (iii) are satisfied up to an error $O(\Delta t)$.

In [19], it has been first remarked that the scheme in [13] can be modified in order to obtain a one-step-scheme replacing p^n in (9) by $(\gamma - 1)\, (E^n - \varepsilon\, \rho^n\, |\mathbf{u}^n|^2/2)$. When $\alpha = 0$, the resulting semi-discrete flux is given by

$$F^{n,n+1} = \left(\mathbf{q}^n, (3 - \gamma)\, \frac{(\mathbf{q}^n)^2}{2\, \rho^n} + \frac{\gamma - 1}{\varepsilon}\, E^{n+1}, \left(\gamma\, E^n - (\gamma - 1)\, \varepsilon \frac{(\mathbf{q}^n)^2}{2\, \rho^n} \right) \frac{\mathbf{q}^{n+1}}{\rho^{n+1}} \right).$$

Then, in one dimension $\partial_x F^{n,n+1} = A_e(W^n, W^{n+1})\, \partial_x W^n + A_i(W^n, W^{n+1})\, \partial_x W^{n+1}$. The eigenvalues of the implicit matrix $A_i(W^n, W^{n+1})$ are $\pm\sqrt{(\gamma - 1)\, (E^n + \tilde{p}^n)/(\rho^{n+1}\, \varepsilon)}$ and 0 where $\tilde{p}^n = (\gamma - 1)\, (E^n - \varepsilon\, \rho^n\, |u^n|^2/2)$. Those of the explicit matrix $A_e(W^n, W^{n+1})$ are $\gamma\, \mathbf{u}^{n+1}$, $(3 - \gamma)\, \mathbf{u}^n/2 \pm \sqrt{(\gamma - 3)\, (\gamma - 1)|\mathbf{u}^n|^2/2}$. So, the explicit operator has complex eigenvalues when $\gamma < 3$ and it cannot be used like that. To recover an explicit matrix A_e with real eigenvalues for all $\gamma \geq 1$, in [19], the following non conservative flux-splitting is proposed

$$F^{n,n+1} = \left(\mathbf{q}^{n+1},\, \rho^n \mathbf{u}^n \otimes \mathbf{u}^n + \frac{1}{\varepsilon}\, p^{n+1}\, \mathrm{Id}_{\mathbb{R}^3}\,,\, \left(\gamma\, E^n - (\gamma - 1)\, \varepsilon \frac{(\mathbf{q}^n)^2}{2\, \rho^n} \right) \frac{\mathbf{q}^{n+1}}{\rho^{n+1}} \right). \tag{10}$$

Note that this flux splitting is also used in [7].

Lemma 2 *We assume impermeability boundary conditions ($u \cdot \nu = 0$ on $\partial\Omega$). The semi-discretization* (6), (10) *satisfies the necessary condition for the asymptotic stability: Property* (i) *of Lemma 1. It does not satisfy Properties* (ii) *and* (iii)*, respectively the asymptotic consistency and the preservation of constant contact discontinuities.*

proof In one dimension $\partial_x F^{n,n+1} = A_e(W^n, W^{n+1})\, \partial_x W^n + A_i(W^n, W^{n+1})\, \partial_x W^{n+1}$. The eigenvalues of $A_e(W^n, W^{n+1})$ are given by $\gamma\, \mathbf{q}^{n+1}/\rho^n$, $(3 - \gamma)\, \mathbf{u}^n$ and those of $A_i(W^n, W^{n+1})$ are 0, $\pm\sqrt{(\gamma - 1)\, (E^n + \tilde{p}^n)/(\rho^n\, \varepsilon)}$. Then, Property (i) is satisfied.

Following the proof of Lemma 1, we obtain $E^{n+1} = \frac{p^{n+1}}{\gamma - 1} = 1/|\Omega| \int_\Omega E^0(x)\, dx$ for all $n \geq 0$. But, we only obtain for all $n \geq 2$, $\nabla \cdot \mathbf{u}^{n+1} = \Delta t\, \nabla \cdot (\mathbf{u}^{n+1}\, \nabla \cdot \mathbf{q}^{n+1}/\rho^n) = O(\Delta t)$. So, the asymptotic consistency is not exact but up to an error of order Δt and (ii) is not satisfied.
Property (iii) is not satisfied in general, since if $\mathbf{u}^{n+1} = \overline{\mathbf{u}}$ and $p^{n+1} = \overline{p}$, the momentum equation gives $\rho^{n+1} = \rho^n - \Delta t\, \overline{\mathbf{u}} \cdot \nabla \rho^n$ while the mass equation gives $\rho^{n+1} = \rho^n - \Delta t\, \overline{\mathbf{u}} \cdot \nabla \rho^{n+1}$. Then, there does not always exist a solution such that $\mathbf{u}^{n+1} = \overline{\mathbf{u}}$ and $p^{n+1} = \overline{p}$.

Let us remark that all considered flux splittings do not perfectly separate pressure and fluid waves. Indeed, the eigenvalues of the implicit part depend on the velocity in each case. It is in fact possible to find such a flux splitting. Let us consider the flux splitting inspired by the operator splitting strategy like in [11]. The semi-discretization consists in an explicit treatment for the transport terms with the fluid velocity:

$$F_e(W) = (\mathbf{q},\, \rho\mathbf{u}\otimes\mathbf{u},\, E\,\mathbf{u}), \qquad F_i(W) = \left(0, \frac{p}{\varepsilon}\,\mathrm{Id}_{\mathbb{R}^3}\,,\, p\,\mathbf{u}\right), \tag{11}$$

Lemma 3 *We assume impermeability boundary conditions ($\mathbf{u}\cdot\nu = 0$ on $\partial\Omega$). The semi-discretization* (6), (11) *satisfies the necessary condition for asymptotic stability and the preservation of constant contact discontinuities: Properties* (i) *and* (iii) *of Lemma 1. It satisfies the asymptotic consistency Property* (ii) *only if the initial velocity is well-prepared for the incompressible limit, more precisely if and only if* $\mathbf{u}(x,0) = \mathbf{u}_0(x) + \sqrt{\varepsilon}\,\overline{\mathbf{u}}_0(x)$ *with* $\nabla\cdot\mathbf{u}_0 = 0$.

proof In one dimension, the eigenvalue of the explicit matrix DF_e is $\mathbf{u}$ of multiplicity 3 and those of the implicit matrix DF_i are 0 and $\pm\sqrt{(\gamma-1)\,c^2/(\gamma\,\varepsilon)}$. Then, Property (i) is satisfied and we can see that this flux splitting perfectly separates the transport and the pressure waves since the eigenvalues of the implicit matrix do no longer depend on u and those of the explicit matrix do not depend on c.

For the asymptotic consistency, following the proof of Lemma 1, we obtain $E^{n+1} = \frac{p^{n+1}}{\gamma-1} = 1/|\Omega|\int_\Omega E^0(x)\,dx = \langle E_0\rangle$ for all $n\geq 0$, but now $\langle E_0\rangle\,\nabla\cdot\mathbf{u}^n(x) + (\gamma-1)\,\langle E_0\rangle\,\nabla\cdot\mathbf{u}^{n+1}(x) = 0$ for all $n\geq 1$. So, we recover Property (ii) if and only if $\nabla\cdot\mathbf{u}^0 = 0$ that is if and only if the initial velocity is well-prepared for the incompressible limit.

In a similar way, we prove that this flux splitting also satisfies Property (iii).

Let us conclude this section with a review of existing low Mach number IMEX schemes using the flux splitting (8). The first article in which (8) has been used for building an all-Mach number scheme is [23]. The scheme is based on staggered grids. In [8] an all-Mach number scheme on collocated grids is presented. The scheme is obtained by discretizing in space the semi-discretization (6), (8). The mass equation can be advanced since the implicit flux is zero on it, then a non-linear system on the momentum and energy has to be solved with a Picard algorithm. The resolution of this non-linear system can be prepared for the low Mach number limit by reformulating it: inserting the expression of q^{n+1} given by the momentum equation into the energy equation, using the state equation and multiplying the result by ε, yields

$$\frac{\varepsilon}{\gamma-1}p^{n+1} - \Delta t^2\nabla\cdot\left(\frac{h^{n+1}}{\rho^{n+1}}\nabla p^{n+1}\right) = \varepsilon E^{n+1,ex} - \varepsilon k_\varepsilon^{n+1} - \varepsilon\Delta t\nabla\cdot\left(\frac{h^{n+1}}{\rho^{n+1}}\mathbf{q}^{n+1,ex}\right), \tag{12}$$

where $k_\varepsilon^{n+1} = k_\varepsilon(W^{n+1}) = \varepsilon\,\rho^{n+1}\,|\mathbf{u}^{n+1}|^2/2$, $h^{n+1} = h(W^{n+1}) = \gamma\,p^{n+1}/(\gamma-1)$ and $\mathbf{q}^{n+1,ex}$ and $E^{n+1,ex}$ are the explicit convected parts given by $\mathbf{q}^{n+1,ex} = \mathbf{q}^n - \Delta t\nabla\cdot(\rho^n\mathbf{u}^n\otimes\mathbf{u}^n)$ and $E^{n+1,ex} = E^n - \Delta t\,\nabla\cdot(k_\varepsilon^n\,\mathbf{u}^n)$. Note that (12) yields an elliptic equation for determining p^{n+1}, but is still coupled with the momentum equation. In [8] this reformulation is done on the fully discretized equations (in time and space) leading to a five points discretization of the diffusion operator on the pressure. To avoid checkerboard effects a non-standard discretization of the enthalpy $\gamma\,p/((\gamma-1)\,\rho$ is introduced and a Picard algorithm is used to solve this non-linear system in terms of p and $\mathbf{q}$. A second-order discretization which is unlimited in time, is also proposed and multi-dimensional (2D and 3D) are performed.

Here, we propose and study an all-Mach number IMEX finite volume scheme also based on the flux splitting (8). However, we prefer discretize the previous reformulated semi-discrete equation instead of the reformulation of the full discrete one thus eliminating the checkerboard effect problems. Moreover, we propose a linearization of this reformulated equation in order to avoid the Picard algorithm for which the convergence is not always guaranteed during the simulations. The resolution is therefore uncoupled, since ρ is calculated first, then p and finally $\mathbf{q}$. Note that, in [9] such a discretization is also proposed and extended to the Navier-Stokes system but the proposed linearization yields an all speed scheme which is not exactly consistent in the limit ε tends to 0, the asymptotic consistency is obtained up to an order Δt term.

Furthermore, we perform a linear stability analysis showing that our scheme is linearly L^2 stable and we propose a second-order in space and time scheme with a limitation process to reduce the oscillations that are common for second-order schemes.

3 Our new first-order AP scheme

3.1 A linear semi-discretization

Our linear first order all-Mach number IMEX semi-discretization consists in replacing in (12) h^{n+1} and k_ε^{n+1} by their values calculated with the explicit convected part of the conservative variables. It is given by

$$\rho^{n+1} = \rho^n - \Delta t \nabla \cdot \mathbf{q}^n, \tag{13a}$$

$$\frac{\varepsilon\, p^{n+1}}{\gamma - 1} - \Delta t^2 \nabla \cdot \left(\frac{h^{n+1,ex}}{\rho^{n+1}} \nabla p^{n+1} \right) = \varepsilon \left(E^{n+1,ex} - k_\varepsilon^{n+1,ex} - \Delta t \nabla \cdot \left(\frac{h^{n+1,ex}}{\rho^{n+1}} \mathbf{q}^{n+1,ex} \right) \right), \tag{13b}$$

$$\mathbf{q}^{n+1} = \mathbf{q}^{n+1,ex} - \Delta t \frac{1}{\varepsilon} \nabla p^{n+1}, \tag{13c}$$

$$E^{n+1} = E^{n+1,ex} - \Delta t \nabla \cdot \left(\frac{\gamma\, p^{n+1}}{(\gamma - 1)\, \rho^{n+1}} \mathbf{q}^{n+1} \right), \tag{13d}$$

where $\mathbf{q}^{n+1,ex} = \mathbf{q}^n - \Delta t \nabla \cdot (\rho^n \mathbf{u}^n \otimes \mathbf{u}^n)$, $E^{n+1,ex} = E^n - \Delta t\, \nabla \cdot (k_\varepsilon^n\, \mathbf{u}^n)$ and $h^{n+1,ex} = \gamma\, (E^{n+1,ex} - k_\varepsilon(W^{n+1,ex}))$.

Note that the scheme is linear and uncoupled since ρ^{n+1}, p^{n+1} , $\mathbf{q}^{n+1}$ and E^{n+1} can be computed sequentially. Moreover, note that we could compute the energy with the state equation (1d) but this leads to non consistent results. In Figure 1, we plot the solution of a Sod shock tube problem at time $t = 0.2$ such that initially $(\rho, u, p)(0, x) = w_L = (1, 0, 1)$ if $x < 0.5$ and $w_R = (0.125, 0, 0.1)$ if $x > 0.5$. The exact solution (see [42]) at time $t = 0.2$ is made up of four constant states (the left state, two intermediate states and the right state) separated by three waves: a rarefaction wave, a contact discontinuity and a shock. In the contact discontinuity, the velocity and pressure being constant, the two intermediate states have the same velocity and pressure. We can see on Figure 1 that the choice of the equation of state to calculate the energy leads to non consistent velocity and pressure for the two intermediate states. The same problem was noticed for the non-linear scheme proposed in [8].

Let us prove that this semi-discretization is asymptotically consistent and preserves the contact discontinuities:

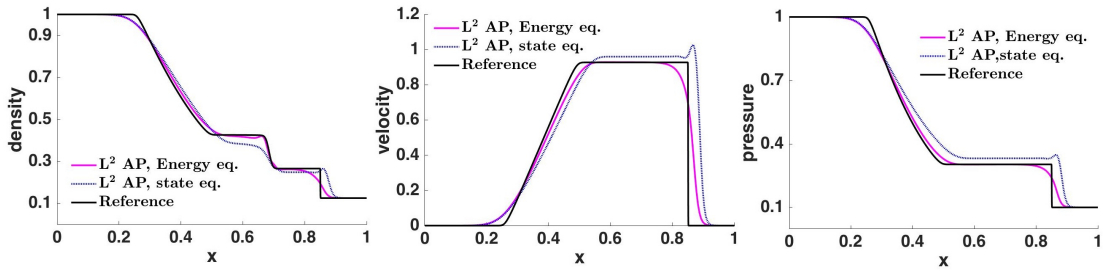

Figure 1: Solution of the Sod shock tube problem at $t_{final} = 0.2$ for 200 cells. Results for our first order AP scheme using the equation of energy (13d) (pink lines) or the equation of state (1d) (black dotted lines) for updating the energy.

Lemma 4 *The semi-discretization* (13) *satisfies Property* (*iii*) *of Lemma 1 and so preserves the constant contact discontinuities.*

Furthermore, if the initial energy is well-prepared for the incompressible limit, more precisely if $E(x,0) = \overline{E}_0 + \varepsilon\,\overline{E}(x)$ *with* $\overline{E}_0$ *constant, and assuming impermeability boundary conditions* ($\mathbf{u}\cdot\nu = 0$ *on* $\partial\Omega$)*, the semi-discretization* (13) *is asymptotically consistent. The formal low Mach number limit of the system gives* $p^{n+1} = (\gamma-1)\,E^{n+1} = (\gamma-1)\,\overline{E}_0$ *and* $\nabla\cdot\mathbf{u}^{n+1} = 0$ *for all* $n \geq 0$.

proof If $\mathbf{u}^n(x) = \overline{\mathbf{u}} \in \mathbb{R}^d$ and $p^n(x) = \overline{p} > 0$ are constant, then the mass equation gives $\rho^{n+1} = \rho^n - \Delta t\,\overline{\mathbf{u}}\cdot\nabla\rho^n$. We have $\mathbf{q}^{n+1,ex} = \rho^{n+1,ex}\,\mathbf{u}^{n+1,ex} = \rho^n\,\overline{\mathbf{u}} - \Delta t\overline{\mathbf{u}}\cdot\nabla\rho^n\,\overline{\mathbf{u}} = \rho^{n+1}\,\overline{\mathbf{u}}$ and $E^{n+1,ex} = E^n - \Delta t\,\varepsilon\,|\overline{\mathbf{u}}|^2/2\,\overline{\mathbf{u}}\cdot\nabla\rho^n = \overline{p}/(\gamma-1) + \varepsilon\,\rho^n\,|\overline{\mathbf{u}}|^2/2 - \Delta t\,\varepsilon\,|\overline{\mathbf{u}}|^2/2\,\overline{\mathbf{u}}\cdot\nabla\rho^n = \overline{p}/(\gamma-1) + \varepsilon\,\rho^{n+1}\,|\overline{\mathbf{u}}|^2/2$ and $h^{n+1,ex} = \overline{p}/(\gamma-1)$. Now, the pressure equation and energy equations lead to $p^{n+1}/(\gamma-1) = \overline{p}/(\gamma-1) - \Delta t\nabla\cdot\left(\gamma\,\overline{p}\,\mathbf{u}^{n+1}\right)$ and $E^{n+1} = \overline{p}/(\gamma-1) + \varepsilon\,\rho^{n+1}\,|\overline{\mathbf{u}}|^2/2 - \Delta t\nabla\cdot\left(\gamma\,\overline{p}\,\mathbf{u}^{n+1}\right)$. So there exists a solution W^{n+1} such that $\mathbf{u}^{n+1} = \overline{\mathbf{u}}$ and $p^{n+1} = \overline{p}$. The semi-discretization (13) preserves constant contact discontinuities.

We perform an asymptotic expansion, assuming that all the quantities $f^l = f_0^l + \sqrt{\varepsilon}\,f_1^l + \varepsilon\,f_2^l$ for $l = n,\ n+1, ex$ or $n+1$ and we prove by induction the asymptotic consistency. We assume $E_0^n = \overline{E}_0$ and we prove $p_0^{n+1} = (\gamma-1)\,E_0^{n+1} = (\gamma-1)\,\overline{E}_0$ and $\nabla\cdot\mathbf{u_0}^{n+1} = 0$.
Inserting the asymptotic expansion into the scheme, we obtain $E_0^{n+1,ex} = E_0^n = \overline{E}_0$, $h_0^{n+1,ex} = \gamma\,E_0^n = \gamma\,\overline{E}_0$, $\mathbf{q}_0^{n+1,ex} = \mathbf{q}_0^n - \Delta t\nabla\cdot(\rho_0^n\mathbf{u}_0^n\otimes\mathbf{u}_0^n)$ and $\nabla p_0^{n+1} = \nabla p_1^{n+1} = 0$. Now, let us remark that using (13c), the pressure equation (13b) can be rewritten

$$\frac{p^{n+1}}{\gamma-1} = E^{n+1,ex} - k_\varepsilon^{n+1,ex} - \Delta t\nabla\cdot\left(\frac{h^{n+1,ex}}{\rho^{n+1}}\mathbf{q}^{n+1}\right).$$

Then, the asymptotic expansion gives

$$\frac{p_0^{n+1}}{\gamma-1} = \overline{E}_0 - \Delta t\nabla\cdot\left(\frac{\gamma\,\overline{E}_0}{\rho_0^{n+1}}\,\mathbf{q}_0^{n+1}\right). \tag{14}$$

Integrating this equation on Ω and using the boundary condition $\mathbf{u}^{n+1}\cdot\nu = 0$ on $\partial\Omega$ we get $p_0^{n+1} = (\gamma-1)\,\overline{E}_0$. Using again (14) gives $\nabla\cdot\mathbf{u}_0^{n+1} = 0$.
Now the energy equation gives

$$E_0^{n+1} = \overline{E}_0 - \Delta t\nabla\cdot\left(\frac{\gamma\,p_0^{n+1}}{(\gamma-1)}\mathbf{u}_0^1\right) = \overline{E}_0 = \frac{p_0^{n+1}}{\gamma-1}.$$

Remark 3 *For non well-prepared initial conditions, it is possible to recover the asymptotic consistency changing the semi-discretization: replacing in* (13d) *the term* $\gamma\, p^{n+1}/(\gamma-1)$ *in the flux by* $h^{n+1,ex}$*. However, this version of the semi-discretization leads to a less diffusive scheme in the* L^2*-stable version of the scheme (see next section) and so oscillations appear in some test-cases. This is why even if the asymptotic consistency is obtained only for well-prepared initial energies we choose to use the semi-discretization* (13)*.*

3.2 The first-order AP schemes

In [18], it has been shown that a centered discretization for the implicit flux terms is sufficient to ensure an L^2 AP-scheme if the explicit flux terms are discretized with an upwind discretization like Roe type solvers. The resulting scheme gives consistent and stable results but can present oscillations which are the signature of the non L^∞-stability. Since the scheme is L^2 stable, these oscillations stay bounded and decrease in time. This problem can be cured introducing an upwinding in the implicit discrete flux leading to the so-called L^∞-AP scheme.

First, let us present the L^2 stable full discretizations in space and time for the previous semi-discretization (13). It is based on the Rusanov solver for the explicit flux F_e and a centered solver for the implicit flux F_i. We consider a uniform discretization in space and time for clarity, with $\Delta x>0$ and $\Delta t>0$ the space and time steps. The fully L^2 stable discrete version of (13) in one dimension reads

$$W_j^{n+1,ex} = W_j^n - \Delta t\,\frac{(\mathcal{F}_e)^n_{j+\frac12}-(\mathcal{F}_e)^n_{j-\frac12}}{\Delta x}, \tag{15a}$$

$$\rho_j^{n+1} = \rho_j^n - \Delta t\frac{(\mathcal{F}_{e\rho})^n_{j+\frac12}-(\mathcal{F}_{e\rho})^n_{j-\frac12}}{\Delta x}, \tag{15b}$$

$$\begin{aligned}\frac{\varepsilon}{\gamma-1}p_j^{n+1} - \frac{\Delta t^2}{\Delta x}\left(\left(\frac{h^{n+1,ex}}{\rho^{n+1}}\right)_{j+\frac12}\frac{p_{j+1}^{n+1}-p_j^{n+1}}{\Delta x} - \left(\frac{h^{n+1,ex}}{\rho^{n+1}}\right)_{j-\frac12}\frac{p_j^{n+1}-p_{j-1}^{n+1}}{\Delta x}\right) \\ = \varepsilon\Big(E_j^{n+1,ex}-k_j^{n+1,ex}\Big) - \varepsilon\frac{\Delta t}{\Delta x}\left(\left(\frac{h^{n+1,ex}}{\rho^{n+1}}\mathbf{q}^{n+1,ex}\right)_{j+\frac12} - \left(\frac{h^{n+1,ex}}{\rho^{n+1}}\mathbf{q}^{n+1,ex}\right)_{j-\frac12}\right),\end{aligned} \tag{15c}$$

$$\mathbf{q}_j^{n+1} = \mathbf{q}_j^{n+1,ex} - \Delta t\,\frac{p_{j+1}^{n+1}-p_{j-1}^{n+1}}{2\varepsilon\Delta x}, \tag{15d}$$

$$E_j^{n+1} = E_j^{n+1,ex} - \frac{\Delta t}{2\Delta x}\left(\left(\frac{\gamma\, p^{n+1}}{(\gamma-1)\,\rho^{n+1}}\mathbf{q}^{n+1}\right)_{j+1} - \left(\frac{\gamma\,\tilde p^{n+1}}{(\gamma-1)\,\rho^{n+1}}\mathbf{q}^{n+1}\right)_{j-1}\right), \tag{15e}$$

where the explicit numerical flux $(\mathcal{F}_e)^n = ((\mathcal{F}_{e\rho})^n, (\mathcal{F}_{eq})^n, (\mathcal{F}_{eE})^n)$ is given by

$$(\mathcal{F}_e)^n_{j+\frac12} = \frac{F_e(W^n_{j+1})+F_e(W^n_j)}{2} - (\mathcal{D}_e)^n_{j+\frac12}(W^n_{j+1}-W^n_j), \tag{15f}$$

where F_e is given by (8) and the explicit viscosity coefficient is taken as half of the maximum explicit eigenvalues of DF_e: $(\mathcal{D}_e)^n_{j+\frac12} = 1/2\,\max\big(|\mathbf{u}^n_{j+1}|, |\mathbf{u}^n_j|\big)$. In the following this scheme is called "L^2 AP" scheme.

Now, we present the scheme with an upwinding on the implicit fluxes. We first compute the L^2 stable solution $W_j^{n+1,L2}$ given by (15) and we add numerical dissipation as done for the explicit numerical flux $(\mathcal{F}_e)_{j+1/2}^n$, thus leading to a modified scheme for the density, momentum and energy equations.

$$W_j^{n+1} = W_j^{n+1,L2} + \frac{\Delta t}{\Delta x}\left((\mathcal{D}_i)_{j+\frac{1}{2}}^n (W_{j+1}^{n+1} - W_j^{n+1}) - (\mathcal{D}_i)_{j-\frac{1}{2}}^n (W_j^{n+1} - W_{j-1}^{n+1})\right), \tag{16}$$

where $(\mathcal{D}_i)_{j+\frac{1}{2}}^n$ is the implicit viscosity coefficient, taken as half of the maximum implicit eigenvalue $(\mathcal{D}_i)_{j+\frac{1}{2}}^n = 1/2 \max\left(|\lambda_i(W_{j+1}^n)|, |\lambda_i(W_j^n)|\right)$ where $|\lambda_i(W)| = |\mathbf{u}|/2 + \sqrt{\mathbf{u}^2/4 + c^2/\varepsilon}$. In the following, this scheme is called "L^∞ AP" scheme.

Remark 4 *1. It is important to note that the upwinding on ρ must be applied after the calculation of the pressure prediction, otherwise we obtain non consistent results for contact discontinuities.*

2. In the numerical results, we will see that this implicit upwinding inversely proportional to $\sqrt{\varepsilon}$ does not seem to degrade the asymptotic consistency of the scheme. However, the results of Lemma 4 are modified since the asymptotic consistency of the semi-discrete model is no longer exact but up to $O(\Delta t)$ terms as shown in the analysis below. We denote by W^{n+1,L^2} and p^{n+1} the solution of the semi-discretized system (13)*. In order to mimic the influence of the implicit upwinding, we consider the following viscous perturbation of* (13) $W^{n+1} = W^{n+1,L^2} + \frac{\Delta t}{\sqrt{\varepsilon}}\Delta W^{n+1}$ *which can be rewritten*

$$\rho^{n+1} = \rho^n - \Delta t \nabla \cdot \mathbf{q}^n + \frac{\Delta t}{\sqrt{\varepsilon}}\Delta\rho^{n+1}, \tag{17a}$$

$$\frac{p^{n+1}}{\gamma - 1} = E^{n+1,ex} - k_\varepsilon^{n+1,ex} - \Delta t \nabla \cdot \left(\frac{h^{n+1,ex}}{\rho^{n+1}}\left(\mathbf{q}^{n+1} - \frac{\Delta t}{\sqrt{\varepsilon}}\Delta q^{n+1}\right)\right), \tag{17b}$$

$$\mathbf{q}^{n+1} = \mathbf{q}^{n+1,ex} - \Delta t \frac{1}{\varepsilon}\nabla p^{n+1} + \frac{\Delta t}{\sqrt{\varepsilon}}\Delta\mathbf{q}^{n+1}, \tag{17c}$$

$$E^{n+1} = E^{n+1,ex} - \Delta t \nabla \cdot \left(\frac{\gamma\, p^{n+1}}{(\gamma-1)\,\rho^{n+1}}\mathbf{q}^{n+1}\right) + \frac{\Delta t}{\sqrt{\varepsilon}}\Delta E^{n+1}, \tag{17d}$$

where $\mathbf{q}^{n+1,ex} = \mathbf{q}^n - \Delta t \nabla \cdot (\rho^n \mathbf{u}^n \otimes \mathbf{u}^n)$, $E^{n+1,ex} = E^n - \Delta t\, \nabla \cdot (k_\varepsilon^n\, \mathbf{u}^n)$ and $h^{n+1,ex} = \gamma\,(E^{n+1,ex} - k_\varepsilon(W^{n+1,ex}))$. We proceed like in the proof of Lemma 4, we use an asymptotic expansion, assuming that all the quantities $f^l = f_0^l + \sqrt{\varepsilon}\, f_1^l + \varepsilon\, f_2^l$ for $l = n,\, n+1, ex$ or $n+1$ and we prove by induction the asymptotic consistency. We assume $E_0^n = \overline{E}_0 + \mathcal{O}(\Delta t)$ and we obtain $p_0^{n+1} = \overline{E}_0 + \mathcal{O}(\Delta t^2)$, $\nabla \cdot \mathbf{u_0}^{n+1} = \mathcal{O}(\Delta t)$ and $E_0^{n+1} = \overline{E}_0 + \mathcal{O}(\Delta t)$.

We also consider the scheme used in [8] slightly modified. Indeed, in [8] the reformulated pressure equation is obtained using the fully discretized scheme giving a discretization of the second-order term in space spread over 5 cells and therefore modified to avoid the well-known checkerboard instabilities. Here, we prefer to discretize the reformulated pressure equation (12) and obtain a discretization of the elliptic term spread over 3 cells. This modification allows for a less diffusive scheme. Furthermore, in [8], the implicit part of the energy flux $\gamma/(\gamma-1)\,p/\rho\ \mathbf{q}$ is discretized as the product of the centered approximations of $\gamma/(\gamma-1)\,p/\rho$ and $\mathbf{q}$, here we prefer to use the

centered approximation of the quantity. This modification improves the convergence of the Picard algorithm. Then, the resulting non-linear (NL) scheme, called "NL L^2 AP" scheme is given by

$$\rho_j^{n+1} = \rho_j^n - \Delta t \frac{(\mathcal{F}_{e\rho})^n_{j+\frac{1}{2}} - (\mathcal{F}_{e\rho})^n_{j-\frac{1}{2}}}{\Delta x}, \tag{18a}$$

$$\begin{aligned}\frac{\varepsilon}{\gamma-1} p_j^{n+1} - \frac{\Delta t^2}{\Delta x}\left(\left(\frac{h^{n+1}}{\rho^{n+1}}\right)_{j+\frac{1}{2}} \frac{p_{j+1}^{n+1} - p_j^{n+1}}{\Delta x} - \left(\frac{h^{n+1}}{\rho^{n+1}}\right)_{j-\frac{1}{2}} \frac{p_j^{n+1} - p_{j-1}^{n+1}}{\Delta x}\right) \\ = \varepsilon\left(E_j^{n+1,ex} - k_j^{n+1}\right) - \varepsilon \frac{\Delta t}{\Delta x}\left(\left(\frac{h^{n+1}}{\rho^{n+1}}\mathbf{q}^{n+1,ex}\right)_{j+\frac{1}{2}} - \left(\frac{h^{n+1}}{\rho^{n+1}}\mathbf{q}^{n+1,ex}\right)_{j-\frac{1}{2}}\right),\end{aligned} \tag{18b}$$

$$\mathbf{q}_j^{n+1} = \mathbf{q}_j^{n+1,ex} - \Delta t\, \frac{p_{j+1}^{n+1} - p_{j-1}^{n+1}}{2\varepsilon \Delta x}, \tag{18c}$$

$$E_j^{n+1} = E_j^{n+1,ex} - \frac{\Delta t}{2\Delta x}\left(\left(\frac{\gamma\, p^{n+1}}{(\gamma-1)\,\rho^{n+1}}\mathbf{q}^{n+1}\right)_{j+1} - \left(\frac{\gamma\, p^{n+1}}{(\gamma-1)\,\rho^{n+1}}\mathbf{q}^{n+1}\right)_{j-1}\right). \tag{18d}$$

We add the same upwinding to the "NL L^2 AP" scheme following the same process. We obtain the "NL L^∞ AP" scheme.

3.3 One-dimensional linear Fourier stability analysis

In all this section, we consider $d = 1$. We linearize the Euler system (1) around a constant solution $\overline{W} = (\overline{\rho}, \overline{q}, \overline{E})$ such that $\overline{\rho} > 0$ and $\overline{p} = (\gamma-1)(\overline{E} - \varepsilon/2\,\overline{q}^2/\overline{\rho}) > 0$. We denote by $\overline{u} = \overline{q}/\overline{\rho}$ and $\overline{c}^2 = \gamma\,\overline{p}/\overline{\rho}$. The linearized system is given by $\partial_t W + A\,\partial_x W = 0$, where $A = DF(\overline{W}) = DF_e(\overline{W}) + DF_i(\overline{W})$.
The eigenvalues of A are $\overline{u} - \overline{c}/\sqrt{\varepsilon}$, $\overline{u}$ and $\overline{u} + \overline{c}/\sqrt{\varepsilon}$. We denote by P the matrix of the eigenvectors of A, then $P^{-1}AP = D$ where D is the diagonal matrix with the eigenvalues of A on the diagonal. We denote by V the coordinates of W in the eigenvectors basis, then $W = PV$ and $\partial_t V + D\,\partial_x V = 0$. Since $\partial_x(DV \cdot V) = (D\partial_x V)\cdot V + (D^t\,\partial_x V)\cdot V = 2\,(D\partial_x V)\cdot V$, taking the scalar product of this equation with V, we obtain $\partial_t \|V\|_2^2(x,t) + \partial_x(DV\cdot V)(x,t) = 0$ where $\|\cdot\|_2$ is the Euclidean norm of $\mathbb{R}^3$. Integrating on the space domain and assuming periodic boundary conditions, we recover $\partial_t \|V\|_{L^2(]0,1[)}(t) = 0$.

Following this proof, using Fourier analysis, we prove the L^2 stability of our "L^2 AP" (15) and "L^∞ AP" (16) schemes. We conclude this section with the same analysis for the non-linear AP scheme "NL L^2 AP" scheme (18). Note that in all three cases we can only explicitly determine one of the three eigenvalues of the amplification matrices. Then, we finish the proof numerically by drawing the solutions of the remaining degree 2 polynomial for values of the Mach number between 0 and 25 (a value large enough to show stability in the low Mach number limit).

We begin, linearizing the semi-discretized system (13) around $\overline{W} = (\overline{\rho}, \overline{\rho}\,\overline{u}, \overline{E})$ a constant solution. Then, we set $W^k = \overline{W} + \epsilon\,\check{W}^k$ for $k = n+1, n$, "$n+1, ex$" and $p^{n+1} = \overline{p} + \epsilon\,\check{p}^{n+1}$. Using Taylor expansions for non-linear terms, neglecting all terms of order greater than ϵ^0, omitting the

"checks" and discretizing the resulting system with the "L^2 AP" scheme, we obtain:

$$W_j^{n+1,ex} = W_j^n - \frac{\Delta t}{\Delta x}\left(DF_e(\overline{W})\,\frac{W_{j+1}^n - W_{j-1}^n}{2} - \frac{\overline{u}}{2}\,(W_{j+1}^n - 2\,W_j^n + W_{j-1}^n)\right), \tag{19a}$$

$$\rho_j^{n+1} = \rho_j^{n+1,ex}, \tag{19b}$$

$$\begin{aligned} p_j^{n+1} - \frac{c^2\,\Delta t^2}{\varepsilon\,\Delta x^2}(p_{j+1}^{n+1} - 2\,p_j^{n+1} + p_{j-1}^{n+1}) &= (\gamma-1)\left(E_j^{n+1,ex} + \varepsilon\,\frac{\overline{u}^2}{2}\,\rho_j^{n+1} - \varepsilon\,\overline{u}\,q_j^{n+1,ex}\right) \\ &\quad - \frac{\Delta t}{\Delta x}\left(-c^2\,\overline{u} + \frac{\gamma\,(\gamma-1)}{2}\,\varepsilon\,\overline{u}^3\right)\,\frac{\rho_{j+1}^{n+1} - \rho_{j-1}^{n+1}}{2} \\ &\quad - \frac{\Delta t}{\Delta x}\left(c^2 - \gamma\,(\gamma-1)\,\varepsilon\,\overline{u}^2\right)\,\frac{q_{j+1}^{n+1,ex} - q_{j-1}^{n+1,ex}}{2} - \frac{\Delta t}{\Delta x}\,\gamma\,(\gamma-1)\,\overline{u}\,\frac{E_{j+1}^{n+1,ex} - E_{j-1}^{n+1,ex}}{2}, \end{aligned} \tag{19c}$$

$$q_j^{n+1} = q_j^{n+1,ex} - \frac{\Delta t}{\varepsilon\,\Delta x}\,\frac{\tilde{p}_{j+1}^{n+1} - p_{j-1}^{n+1}}{2}, \tag{19d}$$

$$E_j^{n+1} = E_j^{n+1,ex} + \frac{\Delta t}{(\gamma-1)\,\Delta x}\left(c^2\,\overline{u}\frac{\rho_{j+1}^{n+1} - \rho_{j-1}^{n+1}}{2} - c^2\,\frac{q_{j+1}^{n+1} - q_{j-1}^{n+1}}{2} - \gamma\,\overline{u}\,\frac{\tilde{p}_{j+1}^{n+1} - p_{j-1}^{n+1}}{2}\right). \tag{19e}$$

where F_e is given by (8). We assume periodic boundary conditions. We have the following result

Lemma 5 (L^2 Stability of our "L^2 AP" scheme) *We denote by $\overline{W} = (\overline{\rho}, \overline{q}, \overline{E})$ the constant solution used for the linearization of the semidiscretization, with $\overline{\rho} > 0$ and $\overline{p} = (\gamma-1)(\overline{E} - \varepsilon/2\,\overline{q}^2/\overline{\rho}) > 0$, $\overline{u} = \overline{q}/\overline{\rho}$ and $\overline{c}^2 = \gamma\,\overline{p}/\overline{\rho}$.*

Let $W_0 \in L^2(]0,1[)$ and $\Delta x > 0$ and $\Delta t > 0$ the space and time steps satisfying the CFL condition $\gamma\,|\overline{u}|\,\Delta t = \Delta x$. We denote by $W_j^0 = 1/\Delta x \int_{(j-1)\,\Delta x}^{j\,\Delta x} W_0(x)\,dx$, by (W_j^n) the solution of system (19), the discretization of the linearized system, and $P\,V^n(x) = W^n(x) = W_j^n = P\,V_j^n$ if $x \in](j-1)\,\Delta x, j\,\Delta x[$ where P is the matrix of the eigenvectors of $DF(\overline{W})$. We set $M_\varepsilon = \sqrt{\varepsilon}\,\overline{u}/\overline{c}$. Then, for all $M_\varepsilon \in]0, 25[$ and all $\gamma \in [1, 10]$, there exists $C > 0$ depending on γ, $\overline{u}$, $\overline{c}$ and ε such that for all $n \geq 0$

$$\|V^n\|_{L^2(]0,1[)} \leq C\,\|V^0\|_{L^2(]0,1[)}.$$

proof We assume $\overline{u} > 0$ for clarity. The same proof can be done for $\overline{u} < 0$.
For $l = n+1$, $n+1, ex$ or n, we set $\hat{W}^l(k) = \int_0^1 W^l(x)\,e^{-2\,i\pi\,k\,x}\,dx$ where W^l is defined on $[0,1[$ by $W^l(x) = W_j^l$ if $x \in [(j-1)\,\Delta x, j\,\Delta x[$ for $j = 1, \cdots, L = 1/\Delta x$. Multiplying Eq. (19a) by P^{-1} and denoting by $V^k = P^{-1}\,W^k$ for $k = n$ or "$n+1, ex$", and taking the Fourier transform, we obtain:

$$\hat{V}^{n+1,ex}(k) = B^e(k)\,\hat{V}^n(k),$$

where $B_e(k) = \Big(\big(1 - \alpha\,\overline{u}\,(1-\cos\varphi)\big)\mathrm{Id}_{\mathbb{R}^3} - \alpha\,i\sin\varphi\,A_e\Big)$ and $\varphi = 2\pi\,k\,\Delta x$, $\alpha = \Delta t/\Delta x$ and

$$A_e = P^{-1}DF_eP = \begin{pmatrix} \frac{\overline{u}}{2} & 0 & -\frac{\overline{u}}{2} \\ \overline{u} - \frac{\overline{c}}{\sqrt{\varepsilon}} & \overline{u} & \overline{u} + \frac{\overline{c}}{\sqrt{\varepsilon}} \\ -\frac{\overline{u}}{2} & 0 & \frac{\overline{u}}{2} \end{pmatrix}, \tag{20}$$

F_e given by (8). The eigenvalues of $B^e(k)$ are given by $\mu_1 = 1 - \alpha\,\overline{u}\,(1-\cos\varphi)$ and $\mu_2 = \mu_3 = 1 - \alpha\,\overline{u}\,(1-\cos\varphi) - i\,\alpha\,\overline{u}\,\sin\varphi$. Under the CFL condition $\alpha\,\overline{u} \leq 1$ or equivalently $\overline{u}\,\Delta t \leq \Delta x$, we clearly

have $|\mu_1| \leq 1$, furthermore $|\mu_{2,3}|^2 = 1 - 2\,\alpha\,\overline{u}\,(1-\cos\varphi)\,(1-\alpha\,\overline{u})$ which is lower than 1 under the same CFL condition. Note that $\hat{\rho}^{n+1} = \hat{\rho}^{n+1,ex}$. Now, the Fourier transforms of Eqs. (19c), (19d) and (19e) give

$$\left(1 + 2\,\alpha^2\,\frac{\overline{c}^2}{\varepsilon}\,(1-\cos\varphi)\right)\hat{p}^{n+1}(k) = \left((\gamma-1)\,\frac{\varepsilon\,\overline{u}^2}{2} - i\,\alpha\,\overline{u}\sin\varphi\left(-\overline{c}^2 + \frac{\gamma\,(\gamma-1)\varepsilon\,\overline{u}^2}{2}\right)\right)\hat{\rho}^{n+1,ex}(k)$$
$$-\left((\gamma-1)\,\varepsilon\,\overline{u} + i\,\alpha\,\sin\varphi\,\left(\overline{c}^2 - \gamma\,(\gamma-1)\,\varepsilon\,\overline{u}^2\right)\right)\hat{q}^{n+1,ex}(k) + (\gamma-1)\,(1 - i\,\alpha\,\overline{u}\,\sin\varphi\,\gamma)\,\hat{E}^{n+1,ex}(k),$$
$$\hat{q}^{n+1}(k) = \hat{q}^{n+1,ex}(k) - \frac{\alpha}{\varepsilon}\,i\sin\varphi\,\hat{p}^{n+1}(k),$$
$$\hat{E}^{n+1}(k) = \hat{E}^{n+1,ex}(k) + \alpha\,i\sin\varphi\,\left(\frac{\overline{c}^2\,\overline{u}}{\gamma-1}\,\hat{\rho}^{n+1} - \frac{\overline{c}^2}{\gamma-1}\,\hat{q}^{n+1} - \frac{\gamma\,\overline{u}}{\gamma-1}\,\hat{p}^{n+1}(k)\right),$$
$$= \hat{E}^{n+1,ex}(k) + \alpha\,i\sin\varphi\,\left(\frac{\overline{c}^2\,\overline{u}}{\gamma-1}\,\hat{\rho}^{n+1} - \frac{\overline{c}^2}{\gamma-1}\,q^{n+1,ex}(k) - \left(-\frac{\overline{c}^2\alpha\,i\sin\varphi}{\varepsilon\,(\gamma-1)} + \frac{\gamma\,\overline{u}}{\gamma-1}\right)\hat{p}^{n+1}(k)\right).$$

Inserting $\hat{p}^{n+1,ex}(k)$ given by the first equation into the second and third one and multiplying the system by P^{-1} yields

$$\hat{V}^{n+1}(k) = B^{im}(k)\,\hat{V}^{n+1,ex}(k) = B^{im}(k)\,B^{e}(k)\,\hat{V}^{n}(k). \tag{21}$$

A quite long calculus gives $det(B^{im}(k)\,B^e(k) - \mu\,\mathrm{Id}_{\mathbb{R}^3}) = (\cos\varphi - i\,\sin\varphi - \mu)\,Q^{im}(\mu)$ where $Q^{im}(\mu)$ is a degree 2 polynomial function whose roots cannot be determined analytically in a simple form because of the dependence of Q^{im} on γ, M_ε, α and φ.

We set $\gamma\,\overline{u}\,\Delta t = \Delta x$ i.e. $\alpha\overline{u} = 1/\gamma < 1$ and we denote by $\mu_{im,1}(M_\varepsilon,\varphi,\gamma)$ and $\mu_{im,2}(M_\varepsilon,\varphi,\gamma)$ the roots of Q^{im} and we plot $\max(\max_{\varphi\in[0,2\,\pi[}|\mu_{im,1}(M_\varepsilon,\varphi,\gamma)|, \max_{\varphi\in[0,2\,\pi[}|\mu_{im,2}(M_\varepsilon,\varphi,\gamma)|)$ (the maximum modulus of the roots of Q^{im}) as a function of $M_\varepsilon \in]0,25]$ and $\gamma \in [1,10]$, we obtain 1 everywhere. Then, for all $M_\varepsilon \in]0,25]$, all $\varphi \in [0,2\,\pi]$ and all $\gamma \in [1,10]$, the spectral radius of $B^{im}B^e$, denoted by $r^i(B^{im}B^e)$, is lower than 1. Since there exists at least one norm matrix $\|\cdot\|$, depending on $B^{im}B^e$, such that $\|B^{im}B^e\| \leq r(B^{im}B^e)$, we obtain $\|\hat{V}^{n+1}\| \leq \|\hat{V}^n\| \leq \cdots \leq \|\hat{V}^0\|$. All norms are equivalent in finite dimension. Then, there exist $C_1 > 0$ and $C_2 > 0$ depending on $\overline{u}$, $\overline{c}$ and ε such that for all $n \geq 0$, $C_1\|V^n\|_{L^2(]0,1[)} = C_1\|\hat{V}^n\|_2 \leq \|\hat{V}^n\| \leq \|\hat{V}^0\| \leq C_2\,\|\hat{V}^0\|_2 = C_2\|V^0\|_{L^2(]0,1[)}$, where $\|\cdot\|_2$ is the Euclidean norm.

Note that this CFL seems to be optimal, indeed for larger values of the CFL, i.e $|\overline{u}|\,\Delta t/\Delta x = C$ with $C > 1/\gamma$, there exists γ such that the spectral radius is bigger than 1.

Let us now perform the stability analysis of the "L^∞ AP" scheme. The "L^∞ AP" scheme on the linearized system consists in the following

$$W_j^{n+1} - \frac{|\lambda_i|\,\Delta t}{2\,\Delta x}\,\left(W_{j+1}^{n+1} - 2\,W_j^{n+1} + W_{j-1}^{n+1}\right) = W_j^{n+1,L2}, \tag{22}$$

where $W_j^{n+1,L2}$ is given by the "L^2 AP" scheme (19) and where $|\lambda_i| = |\overline{u}|/2 + \sqrt{\overline{u}^2/4 + \overline{c}^2/\varepsilon}$. We assume periodic boundary conditions. We prove the following result:

Lemma 6 (L^2 Stability of our "L^∞ AP" scheme) *We denote by $\overline{W} = (\overline{\rho},\overline{q},\overline{E})$ the constant solution used for the linearization of the semidiscretization, with $\overline{\rho} > 0$ and $\overline{p} = (\gamma-1)(\overline{E} - \varepsilon/2\,\overline{q}^2/\overline{\rho}) > 0$, $\overline{u} = \overline{q}/\overline{\rho}$ and $\overline{c}^2 = \gamma\,\overline{p}/\overline{\rho}$.*

Let $W_0 \in L^2(]0,1[)$ and $\Delta x > 0$ and $\Delta t > 0$ the space and time steps satisfying the CFL condition $|\overline{u}|\,\Delta t = \Delta x$. We denote by $W_j^0 = 1/\Delta x\int_{(j-1)\,\Delta x}^{j\,\Delta x} W_0(x)\,dx$, by (W_j^n) the solution of (22) and

$P\,V^n(x) = W^n(x) = W_j^n = P\,V_j^n$ *if* $x \in](j-1)\,\Delta x, j\,\Delta x[$ *where* P *is the matrix of the eigenvectors of* $DF(\overline{W})$. *We set* $M_\varepsilon = \sqrt{\varepsilon}\,\overline{u}/\overline{c}$.
Then, for all $M_\varepsilon \in]0, 25[$ *and all* $\gamma \in [1,5]$, *there exists* $C > 0$ *depending on* γ, $\overline{u}$, $\overline{c}$ *and* ε *such that for all* $n \geq 0$

$$\|V^n\|_{L^2(]0,1[)} \leq C\,\|V^0\|_{L^2(]0,1[)}.$$

proof We assume $\overline{u} > 0$ for clarity. The same proof can be done for $\overline{u} < 0$. We proceed like in the proof of the previous Lemma. We use the coordinates of W in the eigenvector basis of DF and we take the Fourier transform. Using (21), we obtain

$$\beta\,\hat{V}^{n+1}(k) = \left(1 + \alpha\,\overline{u}\,\left(1/2 + \sqrt{1/4 + 1/M_\varepsilon^2}\right)\,(1-\cos\varphi)\right)\,\hat{V}^{n+1}(k) = B^{im}(k)\,B^e(k)\,\hat{V}^n(k).$$

Then, using the results of the proof of the previous Lemma, we obtain

$$det\left(\frac{1}{\beta}\,B^{im}(k)\,B^e(k) - \mu\,\mathrm{Id}_{\mathbb{R}^3}\right) = \frac{1}{\beta^3}\,det\left(B^{im}(k)\,B^e(k) - \beta\,\mu\,\mathrm{Id}_{\mathbb{R}^3}\right)$$
$$= \left(\frac{1 - \alpha\,\overline{u}\,(1 - \cos\varphi + i\,\sin\varphi)}{\beta} - \lambda\right)\overline{Q}^{im}(\lambda),$$

where $\overline{Q}^{im}(\lambda) = \frac{Q^{im}(\beta\,\lambda)}{\beta^2}$. We set $\overline{u}\,\Delta t = \Delta x$ i.e. $\alpha\overline{u} = 1$ and we denote by $\overline{\mu}_{im,1}(M_\varepsilon, \varphi, \gamma)$ and $\overline{\mu}_{im,2}(M_\varepsilon, \varphi, \gamma)$ the roots of $\overline{Q}^i$. We plot $\max(\max_{\varphi\in[0,2\,\pi[}\,|\overline{\mu}_{im,1}(\cdot,\varphi,\cdot)|, \max_{\varphi\in[0,2\,\pi[}\,|\overline{\mu}_{im,2}(\cdot,\varphi,\cdot)|)$ as a function of $M_\varepsilon \in]0, 25]$ and $\gamma \in [1,5]$ that is the maximum modulus of the roots of $\overline{Q}^{im}$, we obtain 1 everywhere. Then, for all $M_\varepsilon \in]0, 25]$, all $\varphi \in [0, 2\,\pi]$ and all $\gamma \in [1,5]$, the spectral radius of $1/\beta\,B^{im}\,B^e$, denoted by $r^i(1/\beta\,B^{im}\,B^e)$, is lower than 1. We conclude like in the proof of Lemma 5.

We conclude this section with the linear stability analysis of the non-linear scheme. We prove that the "NL L^2" AP scheme is L^2 stable. The scheme on the linearized system with periodic boundary conditions, is given by

$$\frac{W_j^{n+1} - W_j^n}{\Delta t} + DF_i(\overline{W})\,\frac{W_{j+1}^{n+1} - W_{j-1}^{n+1}}{2\,\Delta x} + DF_e(\overline{W})\,\frac{W_{j+1}^n - W_{j-1}^n}{2\,\Delta x} - \frac{|\overline{u}|}{2\,\Delta x}\left(W_{j+1}^n - 2\,W_j^n + W_{j-1}^n\right) = 0, \tag{23}$$

for $j = 1, \cdots L = 1/\Delta x$ with $W_0^n = W_L^n$ and $W_{L+1}^n = W_1^n$.

Lemma 7 (Stability of the "NL L^2" AP scheme) *We denote by* $\overline{W} = (\overline{\rho}, \overline{q}, \overline{E})$ *the constant solution used for the linearization of the semidiscretization, with* $\overline{\rho} > 0$ *and* $\overline{p} = (\gamma - 1)(\overline{E} - \varepsilon/2\,\overline{q}^2/\overline{\rho}) > 0$, $\overline{u} = \overline{q}/\overline{\rho}$ *and* $\overline{c}^2 = \gamma\,\overline{p}/\overline{\rho}$.

Let $W_0 \in L^2(]0,1[)$ *and* $\Delta x > 0$ *and* $\Delta t > 0$ *the space and time steps satisfying the CFL condition* $|\overline{u}|\,\Delta t = \Delta x$. *We denote by* $W_j^0 = 1/\Delta x \int_{(j-1)\,\Delta x}^{j\,\Delta x} W_0(x)\,dx$ *and by* (W_j^n) *the solution of* (23) *and* $P\,V^n(x) = W^n(x) = W_j^n = P\,V_j^n$ *if* $x \in](j-1)\,\Delta x, j\,\Delta x[$ *where* P *is the matrix of the eigenvectors of* $DF(\overline{W})$. *We set* $M_\varepsilon = \sqrt{\varepsilon}\,\overline{u}/\overline{c}$.
Then, for all $M_\varepsilon \in]0, 25]$, *there exists* $C > 0$ *depending on* $\overline{u}$, $\overline{c}$ *and* ε *such that for all* $n \geq 0$

$$\|V^n\|_{L^2(]0,1[)} \leq C\,\|V^0\|_{L^2(]0,1[)}.$$

proof We assume $\overline{u} > 0$ for clarity. The same proof can be done for $\overline{u} < 0$.
We proceed like in the proof of the previous lemmas, we multiply (23) by P and we take the Fourier transform, we obtain

$$\hat{V}^{n+1}(k) = \left(\overline{B}^{im}\right)^{-1} B^e \, \hat{V}^n(k),$$

where $\overline{B}^{im} = \mathrm{Id}_{\mathbb{R}^3} + \alpha\, i \sin\varphi\, A_i$, $B^e = \big(1 - \alpha\,\overline{u}\,(1-\cos\varphi)\big) Id - \alpha\, i \sin\varphi\, A_e$ with $A_i = P^{-1} D F_i P$, $A_e = P^{-1} D F_e P$ and $\varphi = 2\pi\, k\, \Delta x$.
The eigenvalues of B^e are $\mu_{e1} = 1 - \alpha\,\overline{u}\,(1-\cos\varphi)$, $\mu_{e2} = \mu_{e3} = 1 - \alpha\,\overline{u}\,(1-\cos\varphi) - i\,\alpha\,\overline{u}\, sin\varphi$. So $|\mu_{ei}| \leq 1 \Leftrightarrow 0 \leq \alpha\,\overline{u} \leq 1$. Those of $\overline{B}^{im}$ are $\mu_{im1} = 1 + i\left(\sin\varphi\,\alpha\,\overline{u}/2 - \alpha\,|\sin\varphi|\,\sqrt{\overline{c}^2/\sqrt{\varepsilon} + \overline{u}^2/4}\right)$, $\mu_{im2} = 1$ and $\mu_{im3} = 1 + i\left(\sin\varphi\,\alpha\,\overline{u}/2 + \alpha\,|\sin\varphi|\,\sqrt{\overline{c}^2/\sqrt{\varepsilon} + \overline{u}^2/4}\right)$, which are all of modulus greater than 1. Now we set $\alpha\,\overline{u} = 1$, and a quite long calculus yields

$$det\left(\left(\overline{B}^{im}\right)^{-1} B_e - \mu\,\mathrm{Id}_{\mathbb{R}^3}\right)) = (\cos\varphi - i\,\sin\varphi - \mu)\, P_2(\mu),$$

where, setting $M_\varepsilon = \sqrt{\varepsilon}\,\overline{u}/\overline{c}$, P_2 is defined by

$$P_2(\mu) = \mu^2 - M_\varepsilon^2\, \frac{2\,\cos\varphi + \sin^2\varphi - i\,\sin\varphi\,(1-\cos\varphi)}{M_\varepsilon^2 + \sin^2\varphi + i\sin\varphi\, M_\varepsilon^2}\; \mu$$
$$+ \frac{M_\varepsilon^4\,(\sin^2\varphi\,\cos\varphi + \cos^2\varphi - i\,\sin\varphi\,\cos\varphi\,(1-\cos\varphi)) + M_\varepsilon^2\,(\sin^2\varphi\,\cos^2\varphi - i\,\sin^3\varphi\,\cos\varphi)}{(M_\varepsilon^2 + \sin^2\varphi + i\sin\varphi\, M_\varepsilon^2)^2}.$$

We denote by $\mu_1(M_\varepsilon, \varphi)$ and $\mu_2(M_\varepsilon, \varphi)$ the roots of P_2 and we plot on Figure 2, on the left: the maximum modulus of the roots of P_2 that is $\max(|\mu_1(M_\varepsilon,\varphi)|, |\mu_2(M_\varepsilon,\varphi)|)$ as a function of $\varphi \in [0, 2\,\pi]$ and $M_\varepsilon \in]0, 25]$, on the right $\max(\max_{\varphi\in[0,2\,\pi[}\,|\mu_1(M_\varepsilon,\varphi)|, \max_{\varphi\in[0,2\,\pi[}\,|\mu_2(M_\varepsilon,\varphi)|)$ as a function of $M_\varepsilon \in]0, 25]$.

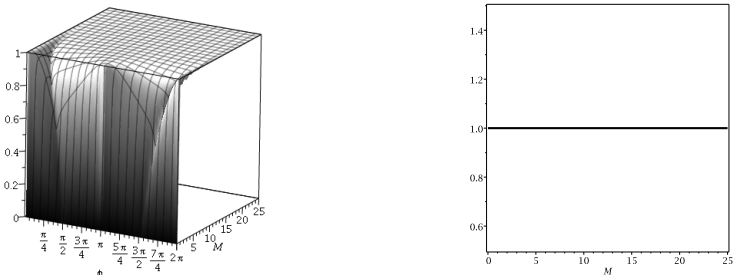

Figure 2: Maximum modulus of the roots of P_2.

Then for all $M_\varepsilon \in]0, 25]$ and all $\varphi \in [0, 2\,\pi]$, the spectral radius of $\left(\overline{B}^{im}\right)^{-1} B^e$, denoted by $r\left(\left(\overline{B}^{im}\right)^{-1} B^e\right)$, is lower than 1. We conclude like in the proof of Lemma 5.
Note that when $\varepsilon = 0$, P_2 reduces to μ^2 and when $\sin\varphi = 0$, it reduces to $\mu^2 - 2\,\cos\varphi\,\mu + \cos^2\varphi$. In this last case, $B^{im} = \big(\mathrm{Id}_{\mathbb{R}^3} + \alpha\, 2\, i \sin\varphi\, A_i\big) = \mathrm{Id}_{\mathbb{R}^3}$ and so the eigenvalues of $(B^{im})^{-1} B^e$ are those of B^e which when $\alpha\overline{u} = 1$ and $\sin\varphi = 0$, are given by $\mu_{e1} = \mu_{e2} = \mu_{e3} = \cos\varphi = 1$.

3.4 Numerical results for the first-order AP schemes

In this section, we present several numerical test-cases which show the good behavior of our new linear first-order AP schemes given by (15), (16). We compare it to the non-linear AP scheme (18) inspired by [8]. If not mentioned, the reference solution is computed using a first-order Rusanov explicit scheme on a refined grid ($N_x = 3000$). For all test-cases the space domain is set to $\Omega = [0; 1]$ and we choose $\gamma = 1.4$. If not mentioned $\varepsilon = 1$.

3.4.1 Classical Riemann problems: The Sod and Lax problems

The initial data of the classical Riemann problems is given by $(\rho, u, p)(0, x) = w_L = (\rho_L, u_L, p_L)$ if $x < 0.5$ and $w_R = (\rho_R, u_R, p_R)$ otherwise, where $t_{final} = 0.2$, $\rho_L = 1$, $u_L = 0$, $p_L = 1$, $\rho_R = 0.125$, $u_R = 0$ and $p_R = 0.1$ for the Sod problem and $t_{final} = 0.14$, $\rho_L = 0.445$, $u_L = 1.698$, $p_L = 3.528$, $\rho_R = 0.5$, $u_R = 0$ and $p_R = 0.571$ for the Lax problem. For both test-cases, the numerical results are compared to the exact solution.
The Sod and Lax problems are benchmarks in gas dynamics [42]. Their solutions consist of a left-moving rarefaction fan, an intermediate contact discontinuity and a right-moving shock wave, see Figure 3 and Figure 5.
For the Sod problem see Figure 3, the Mach number, $M^2 = u^2\,\rho/(\gamma\,p)$, ranges from 0 to 1 since at $x = 0$ or $x = 1$, $M = 0$ and at $x = 0.5$, $M \approx 0.9$. For the Lax problem, it ranges between 0 and 1.2. We can see that our new linear AP scheme gives similar results to the "NL AP" schemes for both L^2 and L^∞ versions. For the Sod problem, at the contact wave, we can see a small overshoot in the density for our "L^2 AP" scheme which is also present but less important for the "NL L^2 AP" scheme. This overshoot disappears when the mesh is refined see Figure 4.
Note that the position of the right moving shock wave in the pressure or in the velocity seems not well captured by all the schemes in Figure 3, but when we refined the mesh, we can see the convergence of the scheme to the right position of the shock, see Figure 4.

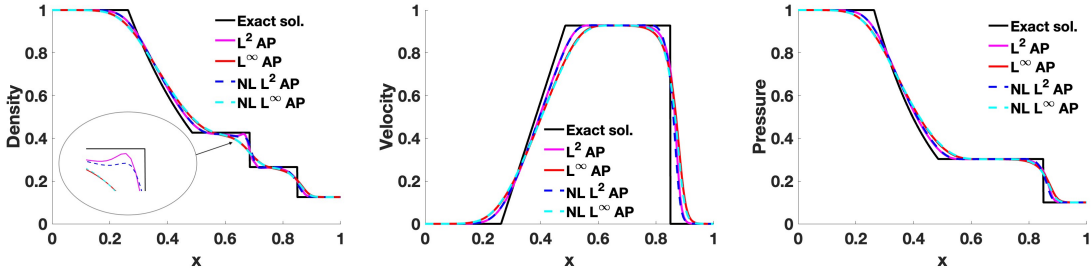

Figure 3: Sod problem for 200 cells. Comparison of our "L^2 AP" and "L^∞ AP" schemes (solid lines) with the "NL L^2 AP" and "NL L^∞ AP" schemes (dashed lines).

Furthermore, for the Lax problem, Figure 5, we can see on the density, that the linear schemes are more diffusive than the non linear schemes again at the contact wave. These differences disappear when the mesh is refined see Figure 6. We can also see that the constant pressure and velocity contact are well approximated in the contact wave.

The linearization of the non-linear system alter the results only slightly. Note that the implicit upwinding, necessary to obtain the L^∞ stability property, introduces numerical diffusion as it is

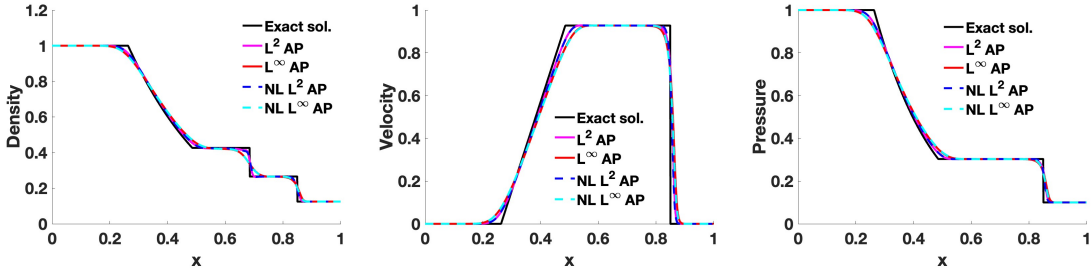

Figure 4: Sod problem for 500 cells. Comparison of our "L^2 AP" and "L^∞ AP" schemes (solid lines) with the "NL L^2 AP" and "NL L^∞ AP" schemes (dashed lines).

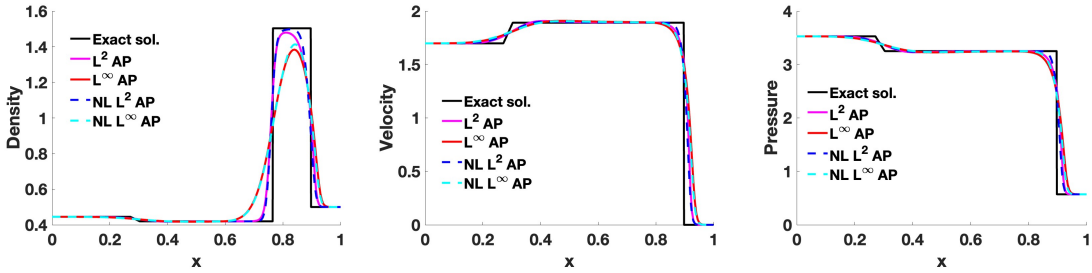

Figure 5: Lax problem for 200 cells. Comparison of our "L^2 AP" and "L^∞ AP" schemes (solid lines) with the "NL L^2 AP" and "NL L^∞ AP" schemes (dashed lines).

expected and does not appear to be necessary in these test-cases. We will see in the next test-case that without this upwinding, non-physical oscillations may appear.

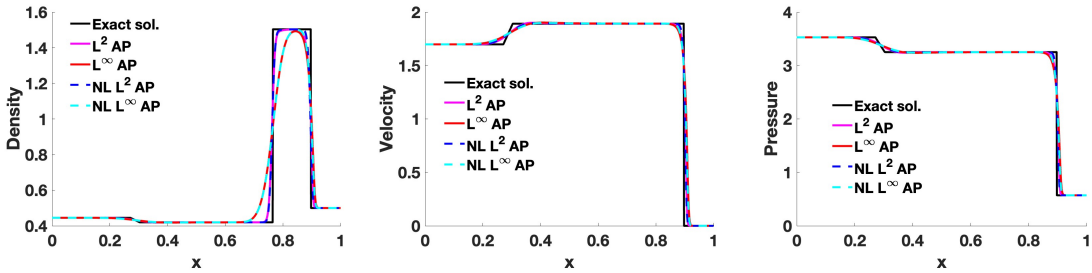

Figure 6: Lax problem for 500 cells. Comparison of our "L^2 AP" and "L^∞ AP" schemes (solid lines) with the "NL L^2 AP" and "NL L^∞ AP" schemes (dashed lines).

3.4.2 Several interacting Riemann problems

In this section, we consider the test-case introduced in [15] which consists in several interacting Riemann problems. Shocks and contact discontinuities are stronger when ε is bigger. The initial

data is given by $\rho(x,0) = 1$, $p(0,x) = 1$, $u(x,0) = 1 - \varepsilon/2$ if $x \in [0, 0.2[\cup]0.8, 1]$, 1 if $x \in [0.2, 0.3] \cup [0.7, 0.8]$ and $1 + \varepsilon/2$ if $x \in]0.3, 0.7[$. The system is supplemented with periodic boundary conditions. This test-case is particularly singular for first-order AP schemes, which all exhibit non-physical oscillations on the density when the CFL is not reduced. The objective is to test the limits of the schemes and to show that the L^∞ corrections are necessary even if they are not perfect. Following the linear stability analysis, between times t^n and t^{n+1}, we set the following CFL for the schemes:

– For the "L^∞" AP, "NL L^2" AP, "NL L^∞" AP schemes : $\Delta t \leq cfl\, \Delta x / \max_j |u_j^n|$,

– For the "L^2 AP" scheme : $\Delta t \leq cfl\, \Delta x / (\gamma \max_j |u_j^n|)$,

where $cfl \leq 1$ is a given positive real number.

The results are given for different values of the Mach number: $\varepsilon = 1$, $\varepsilon = 10^{-1}$ and $\varepsilon = 10^{-2}$ respectively in Figures 7, 8, 9. We only show the density since the oscillations do not appear on the velocity and pressure. In each corresponding regime we observe oscillations on the density profile for all schemes. These non physical oscillations are more important in the L^2 versions of the schemes and decrease with the cfl number. When using the L^∞ discretizations, these oscillations are significantly reduced. This illustrates the need to add the upwinding on the L^2 discretization. Therefore, for the rest of the paper we will keep only the "L^∞ AP" scheme called "Order 1 AP" scheme.

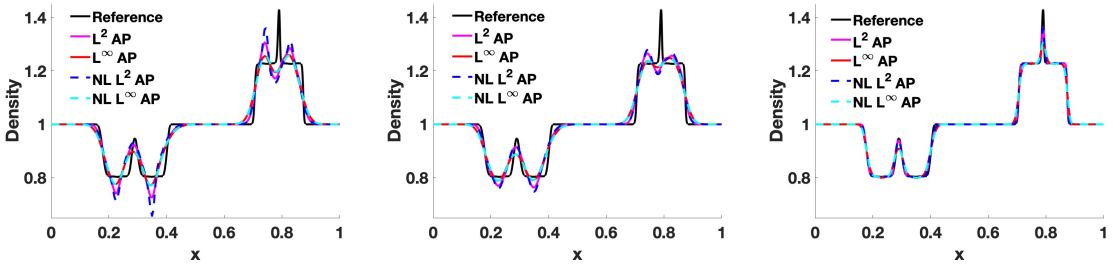

Figure 7: Several interacting Riemann problems test-case, $\varepsilon = 1$, $t_{final} = 0.04$. Left: cfl=0.9 with 200 cells, Middle: cfl=0.5 with 200 cells, Right: cfl=0.1 with 1000 cells

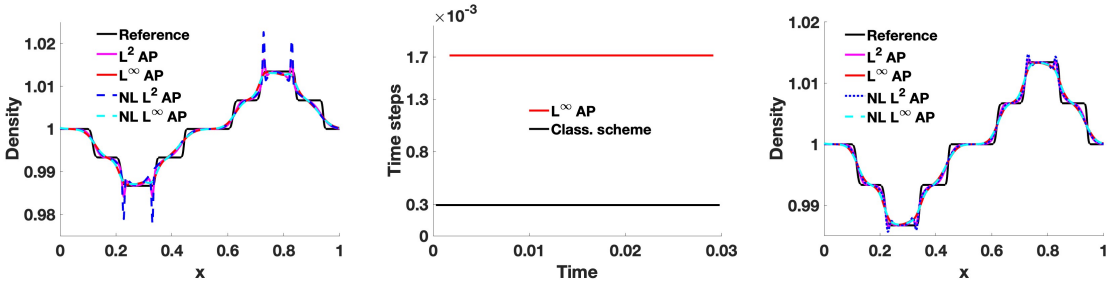

Figure 8: Several interacting Riemann problems test-case, $\varepsilon = 10^{-1}$, $t_{final} = 0.03$ with 500 cells. Left and Middle: cfl=0.9 Right: cfl=0.5

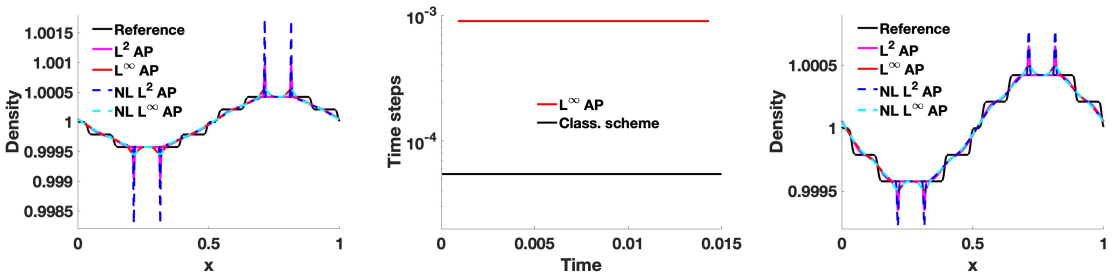

Figure 9: Several interacting Riemann problems test-case, $\varepsilon = 10^{-2}$, $t_{final} = 0.015$ with 1000 cells. Left and Middle: cfl=0.9 Right: cfl=0.5

In Figures 8 and 9 (center plot), in order to show the asymptotic stability of our scheme, we compare the time steps of our L^∞ AP scheme against the classical explicit one. For both picture, we can see that the ratio between the time step of the "L^∞ AP" scheme and the classical explicit scheme is greater than the expected gain $\sqrt{\varepsilon}$.

4 Low oscillating second-order AP-scheme

In this section, we extend our new linear AP scheme to second-order accuracy in time and space. Like in [18, 8], this extension is based on an Implict-Explicit (IMEX) Runge-Kutta approach [3, 39, 20, 6]. In particular, we make use of the second-order Ascher, Ruuth and Spiteri [3] scheme denoted in the sequel by ARS(2,2,2) which have been shown in [36] to be the better choice for second-order discretizations. We recall (see [25]) that implicit methods of order higher than one for hyperbolic problems cannot be strong stability preserving (SSP), i.e. they cannot maintain the strong stability in the same norm as the first-order scheme. In our case that means that we cannot build a high-order scheme which preserves the TVD or L^∞ stabilities of the first-order schemes and this situation does not change when IMEX methods are employed [18]. To bypass this limitation, we use the same approach as in [18] for the isentropic Euler equations. The idea consists in blending together first and second-order implicit time-space discretizations giving rise to less diffusive first-order AP-scheme which guarantees the preservation of the L^∞ stability and TVD property and, to use the second-order scheme as often as possible by setting up a MOOD (Multidimensional Optimal Order Detection) method [12]. We detail in the next sections the different steps of the scheme.

4.1 Second-order AP semi-discretization in time

First, let us present the second-order semi-discretization in time. Using the ARS(2,2,2) and setting $\beta = 1 - 1/\sqrt{2}$, the following second-order in time scheme is obtained

$$\frac{W^\star - W^n}{\Delta t} + \beta\,\nabla\cdot F_e(W^n) + \beta\,\nabla\cdot F_i(W^\star) = 0,$$
$$\frac{W^{n+1} - W^n}{\Delta t} + \nabla\cdot F(W^\star) + (1-\beta)\nabla\cdot(F_e(W^\star) - F_e(W^n)) + \beta\nabla\cdot(F_i(W^{n+1}) - F_i(W^\star)) = 0.$$

Following the reformulation and linearization used for the first-order AP scheme, we obtain

$$\rho^\star = \rho^n - \beta\Delta t\nabla\cdot\mathbf{q}^n, \tag{24a}$$
$$\frac{\varepsilon}{\gamma-1}p^\star - \beta^2\Delta t^2\nabla\cdot\left(\frac{h^{\star,ex}}{\rho^\star}\nabla p^\star\right) = \varepsilon\left(E^{\star,ex} - k^{\star,ex}\right) - \varepsilon\beta\Delta t\nabla\cdot\left(\frac{h^{\star,ex}}{\rho^\star}\mathbf{q}^{\star,ex}\right), \tag{24b}$$
$$\mathbf{q}^\star = \mathbf{q}^{\star,ex} - \beta\Delta t\frac{1}{\varepsilon}\nabla p^\star, \tag{24c}$$
$$E^\star = E^{\star,ex} - \beta\Delta t\nabla\cdot\left(\frac{\gamma p^\star}{(\gamma-1)\rho^\star}\mathbf{q}^\star\right), \tag{24d}$$

where $\mathbf{q}^{\star,ex} = \mathbf{q}^n - \beta\Delta t\nabla\cdot(\rho^n\mathbf{u}^n\otimes\mathbf{u}^n)$, $E^{\star,ex} = E^n - \beta\Delta t\,\nabla\cdot(k_\varepsilon^n\,\mathbf{u}^n)$ and $h^{\star,ex} = \gamma\,(E^{\star,ex} - k_\varepsilon(W^{\star,ex})$ and

$$\rho^{n+1} = \rho^n - \Delta t\,((\beta-1)\nabla\cdot\mathbf{q}^n + (2-\beta)\nabla\cdot\mathbf{q}^\star)\,, \tag{25a}$$

$$\frac{\varepsilon}{\gamma-1}p^{n+1} - \beta^2\Delta t^2\nabla\cdot\left(\frac{h^{n+1,ex}}{\rho^{n+1}}\nabla p^{n+1}\right) \tag{25b}$$

$$= \varepsilon\left(E^{n+1,ex} - k^{n+1,ex}\right) - \varepsilon\beta\Delta t\nabla\cdot\left(\frac{h^{n+1,ex}}{\rho^{n+1}}\mathbf{q}^{n+1,ex}\right),$$

$$\mathbf{q}^{n+1} = \mathbf{q}^{n+1,ex} - \frac{\beta\Delta t}{\varepsilon}\nabla p^{n+1}, \tag{25c}$$

$$E^{n+1} = E^{n+1,ex} - \beta\Delta t\nabla\cdot\left(\frac{\gamma p^{n+1}}{(\gamma-1)\rho^{n+1}}\mathbf{q}^{n+1}\right), \tag{25d}$$

with $h^{n+1,ex} = \gamma\,(E^{n+1,ex} - k_\varepsilon(W^{n+1,ex}))$ and $W^{n+1,ex} = (\rho^{n+1}, \mathbf{q}^{n+1,ex}, E^{n+1,ex}) = W^n - \Delta t\,((\beta-1)\nabla\cdot F_e(W^n) + (2-\beta)\nabla\cdot F_e(W^\star) + (1-\beta)\nabla\cdot F_i(W^\star))$.

Let us prove the asymptotic consistency of this semi-discretization

Lemma 8 *If the initial energy is well-prepared for the incompressible limit, more precisely if $E(x,0) = \overline{E}_0 + \varepsilon\,\overline{E}(x)$ with $\overline{E}_0$ constant, and assuming impermeability boundary conditions ($\mathbf{u}\cdot\nu = 0$ on $\partial\Omega$), the second-order semi-discretization* (24)-(25) *is asymptotically consistent. The formal low Mach number limit of the system gives $p^{n+1} = (\gamma-1)\,E^{n+1} = (\gamma-1)\,\overline{E}_0$ and $\nabla\cdot\mathbf{u}^{n+1} = 0$ for all $n \geq 0$.*

proof We proceed like in the proof of Lemma 4, we perform an asymptotic expansion, assuming that all the quantities $f^l = f_0^l + \sqrt{\varepsilon}\,f_1^l + \varepsilon\,f_2^l$ for $l = n, n+1, ex, \star$ or $n+1$ and we prove by induction the asymptotic consistency. We assume $E_0^n = \overline{E}_0$ and we prove $\nabla p_0^{n+1} = (\gamma-1)\,E_0^{n+1} = 0$ and $\nabla\cdot\mathbf{u_0}^{n+1} = 0$. The first step (24) gives $E^{\star,ex} = \overline{E}_0$, $h^{\star,ex} = \gamma\,\overline{E}_0$, $p_0^\star = \nabla p_1^\star = 0$. Then inserting (24c) into (24b), and performing the asymptotic expansion of the variables, gives $p_0^\star = (\gamma-1)\,\overline{E}_0 = (\gamma-1)\,\overline{E}_0$ and $\nabla\cdot u_0^\star = 0$. The energy yields $E_0^\star = \overline{E}_0$. For the second step (25), we proceed similarly using in addition the results of the first step.

4.2 Second-order discretization in space

In order to extend the space accuracy to second-order, we use classically the MUSCL technique and so a piecewise linear reconstruction of W_j^n given by $\widehat{W}_j^n(x) = W_j^n + \sigma_j^n(x - x_j)$ where σ_j^n is a limited slope and is computed using a minmod limiter (see [18] for more details). This piecewise linear reconstruction is used for defining the numerical flux at the interfaces using the notations introduced for the first-order AP scheme

$$(\mathcal{F}_e)_{j+1/2}^n := \frac{F_e(W_{j+1,-}^n) + F_e(W_{j,+}^n)}{2\Delta x} - (\mathcal{D}_e)_{j+1/2}^n(W_{j+1,-}^n - W_{j,+}^n), \tag{26}$$

where $(\mathcal{D}_e)_{j+1/2}^n = 1/2\,\max\left(|\mathbf{u}_{j,+}^n|, |\mathbf{u}_{j+1,-}^n|\right)$ and where $W_{j,\pm}^n = \widehat{W}_j^n(x_j \pm \Delta x/2) = W_j^n \pm \Delta x/2\,\sigma_j^n$. For the sake of simplicity, we carry out the reconstruction of variables only for the explicit flux $(\mathcal{F}_e)^n$ and not for the implicit terms in the calculation of the pressure prediction. Moreover numerical tests intend to show that adding implicit diffusion only at the end of the second step is sufficient. As done for the Order 1 "L^∞ AP" scheme, we compute the L^2 stable solution $W_j^{n+1,L2}$ with (24)-(25),

(26) (the scheme is called "Order 2 L^2 AP" scheme) and then add numerical dissipation on the conservative variables:

$$W_j^{n+1} = W_j^{n+1,L2} + \frac{\beta\Delta t}{\Delta x}\left((\mathcal{D}_i)^n_{j+1/2}(\tilde{W}^{n+1}_{j+1,-} - \tilde{W}^{n+1}_{j,+}) - (\mathcal{D}_i)^n_{j-1/2}(\tilde{W}^{n+1}_{j,-} - \tilde{W}^{n+1}_{j-1,+})\right), \quad (27)$$

where $(\mathcal{D}_i)^n_{j+1/2} = 1/2\,\max\left(|\lambda_i(W^n_{j+1,-})|, |\lambda_i(W^n_{j,+})|\right)$, and $\tilde{W}^{n+1}_{j,\pm} = W^{n+1}_j \pm \frac{\Delta x}{2}\sigma^n_j$. This scheme is called "Order 2 L^∞ AP" scheme.

4.3 The first-order TVD AP scheme

It is well known that a second-order discretization in space introduces oscillations which can be eliminated by using limiters. The same problem occurs with the time discretization. Indeed, using this second-order discretization in time with a first-order discretization in space leads to numerical results with oscillations: on Figure 10, we can see that the Order 2 AP scheme gives more accurate results than the first-order AP scheme but we can also remark that when the Mach number decreases oscillations appear. In [18], it has been proved that these oscillations are the result of the loss of the L^∞ stability and TVD properties of the second-order semi-discretization. These properties can be recovered only if time steps are of the order of that of the explicit semi-discretization and so constrained by the Mach number. It has been shown in [25] that there does not exist TVD implicit Runge-Kutta schemes with unconstrained time steps of order higher than one for an hyperbolic equation.

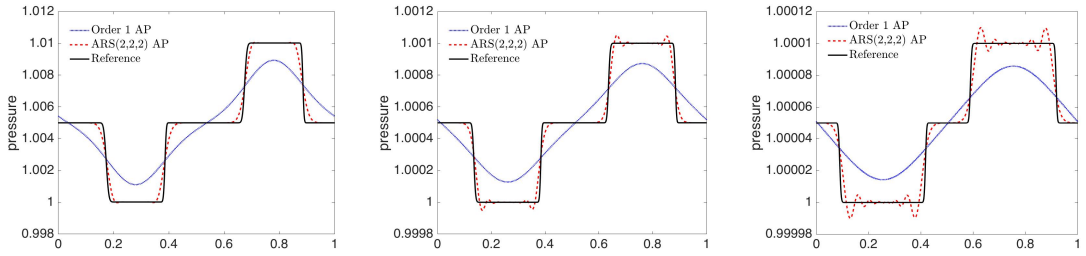

Figure 10: Shock tube test-case: $\rho(0,x) = 1$, $u(0,x) = 1$, $p(0,x) = 1 + \varepsilon$ if $x < 0.5$, 1 otherwise. Results for different Mach numbers: $\varepsilon = 10^{-2}$ (left), $\varepsilon = 10^{-3}$ (center) and $\varepsilon = 10^{-4}$ (right). Comparison of the approximated pressure given by the first-order "L^∞ AP" and second-order in time AP schemes against the reference solution.

To tackle this problem and obtain a L^∞ stable and TVD numerical semi-discretization less diffusive than the Order 1 AP scheme "L^∞ AP" scheme, we introduce a convex combination between the first and second order AP schemes, as proposed in [18] for the isentropic Euler equations:

$$W^{n+1} = (1-\theta)W^{n+1,O1} + \theta W^{n+1,O2}, \quad (28)$$

where $W^{n+1,O1}$ is given by the "L^∞ AP" scheme (13), $W^{n+1,O2}$ by the second-order AP scheme (24)-(25) and $\theta \in [0,1]$ is set to $\beta/(1-\beta)$, proved in [18] to be the largest possible value to ensure the TVD property in the case of an advection equation. In the following, this scheme is referred as the "TVD-AP" scheme. Note that this TVD-AP scheme is less diffusive but it is still a first-order

scheme. We will see in Section 4.8, how we can bypass this limitation. Furthermore, since it is a combination of the first and second-order schemes which are both asymptotically consistent, it is also asymptotically consistent.

4.4 Numerical convergence: The 2D isentropic vortex

The isentropic vortex problem was initially introduced by [29] to test the accuracy of numerical methods since the analytical solution is regular and known. It corresponds to a flow characterized by $(\rho_\infty, u_\infty, v_\infty, p_\infty) = (1, 1, 1, 1)$ to which we add an isentropic vortex given by perturbations on (u, v) and the temperature $T = p/\rho$, but no perturbation on the entropy $S = p/\rho^\gamma$: $(\delta u, \delta v) = d/(2\pi)e^{\frac{1-r^2}{2}}(-y, x)$, $\delta T = -(\gamma-1)d^2/(8\gamma\pi^2)\, e^{1-r^2}$, $\delta S = 0$, where $\gamma = 1.4$, $r = \sqrt{x^2+y^2}$ and the vortex strength $d = 5$. The initial data is given by $(\rho, u, v, p)(0, x, y) = (\rho_\infty + \delta\rho, u_\infty + \delta u, v_\infty + \delta v, p_\infty + \delta p)$, where the perturbations for the density and pressure read $\delta\rho = (1+\delta T)^{1/(\gamma-1)} - 1$ and $\delta p = (1+\delta T)^{\gamma/(\gamma-1)} - 1$. The domain is set to $\Omega = [-5; 5]^2$ and periodic boundary conditions are used. The exact solution of this problem with the above initial data is the initial vortex convected with the mean velocity i.e. $W(t, x, y) = W_0(x - u_\infty t, y - v_\infty t)$. To assess the numerical order of accuracy, we compute the relative L^2 errors for several uniform meshes: $e_{L2} = ||\rho^n - \rho^n_{ex}||_{L^2}/||\rho^n_{ex}||_{L^2}$. The L^2 errors of the density are computed at $t_{final} = 1$ and are shown in logarithmic scale as a function of the number of cells on Figure 11 on the right. We get the expected orders for each of the schemes. Note that the TVD AP scheme is a first order scheme but with an error always lower than the first-order schemes, which confirms that the numerical diffusion has been decreased.

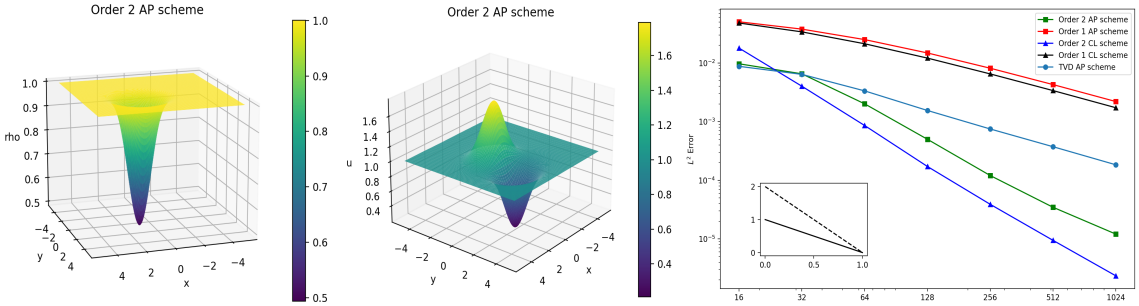

Figure 11: Left and middle panels: Density and first component of the velocity given by the Order 2 AP scheme with 128×128 grid points. Right panel: L^2 norm of the density error at time $t_{final} = 1$ given by the Order 1 "L^2 AP" scheme and the "Order 2 L^2 AP" scheme with no minmod limitation for the calculation of the slopes (squares) and the first and second orders explicit schemes (triangles) and by the "TVD AP" scheme (dots) as functions of the number of cells in logaritm scale.

4.5 The Gresho vortex

The Gresho vortex is a standard test-case (see for instance [9], [23]) to assess the AP property of a scheme as well as to quantify the loss of kinetic energy for different Mach number regimes. The

solution, written in polar coordinates, reads

$$(\rho(r), u_\varphi(r), p(r)) = \begin{cases} (1\,,\, 5\,r\,,\, p_0 + 12.5\,r^2), & \text{if } 0 \le r < 0.2, \\ (1\,,\, 2 - 5\,r\,,\, p_0 + 12.5\,r^2 + 4\,[1 - 5\,r - \ln(0.2) + \ln(r)]), & \text{if } 0.2 \le r < 0.4, \\ (1, 0, p_0 - 2 + 4\,\ln(2), & \text{if } r \ge 0.4 \end{cases}$$

where $u_\varphi(r)$ is the angular velocity, $r = \sqrt{(x-0.5)^2 + (y-0.5)^2}$ is the radius on the computational domain $\Omega = [0,1] \times [0,1]$ and $p_0 = \rho/(\gamma\, M^2)$ depends on the physical Mach number. The density is constant and the divergence-free velocity field can be obtained from u_φ as $\mathbf{u} = (u, v) = u_\varphi\,(-\sin(\varphi), \cos(\varphi))$ with $\varphi = \arctan\left(\frac{y-0.5}{x-0.5}\right)$. In Figure 12, we show on the left, the physical Mach number distribution $|\mathbf{u}|/c$ where $c = \sqrt{\gamma\, p/\rho}$, the results are given by the "Order 2 L^2 AP" scheme for different values of M after a full turn of the vortex at $t = 0.4\,\pi$ and for a grid of 80×80 cells. We see that our scheme is able to preserve the initial distribution (first subfigure) independently of the Mach number regime unlike classical discretizations for which the dissipation is related to M. On the right pictures of Figure 12, we focus on the pressure profile in the x and y direction and compare it against the initial condition. We can see that, even for $M = 10^{-3}$, our scheme is able to capture the pressure perturbations and does not show any oscillation.
To further check the asymptotic accuracy of our scheme we show in Figure 13 the ratio between the kinetic energy at each time step $k(t)$ and the initial kinetic energy $k(0)$ for the Mach numbers $M = 10^{-1}, 10^{-2}, 10^{-3}$ and two grid resolutions 40×40 and 80×80. The results are given for the Order 2 L^2 AP scheme with no limiter in space (left) and with the minmod limiter (right). We see in the graphs that for a same grid resolution the lines for the different Mach numbers are overlapping which shows that the loss of kinetic energy is independent of the chosen Mach number regime. Comparing the two subfigures we see that the loss is mostly due to the limiter in space, 0.9825 (unlimited) against 0.92 (limited) for the coarser grid.

4.6 A 2D Riemann problem

We consider a two-dimensional Riemann problem introduced in [10]. We set $\Omega = [-0.5, 0.5]^2$ and transmissive boundary conditions $\nabla W \cdot \nu = 0$. We set $\mathbf{q} = \rho\,\mathbf{u} = \rho\,(u, v)$. The initial data consists in four constant states defined in four quadrants given by

$$(\rho, u, v, p)(0, x, y) = \begin{cases} (1,\ 0.726,\ 0,\ 1), & \text{if } x < 0, y > 0, \\ (0.5313,\ 0,\ 0,\ 0.4), & \text{if } x > 0, y > 0, \\ (0.8,\ 0,\ 0,\ 1), & \text{if } x < 0, y \le 0 \\ (1,\ 0,\ 0.726,\ 1), & \text{if } x > 0, y < 0. \end{cases}$$

We set $\varepsilon = 1$, but we will see that the physical Mach number $|\mathbf{u}|/c$ where $c = \sqrt{\gamma\, p/\rho}$, ranges between 0 and 1.14. The solution at each time $t > 0$ is constituted of two shocks moving respectively towards the right and top of the domain and two steady contact discontinuities in the bottom left part of the domain.
We use two different schemes: the "Order 2 L^2 AP" scheme (24)-(25), (26) and the "Order 2 L^∞ AP" scheme (27). In Figure 14, we display on the left and middle, the density isolines at the final time $T = 0.25$. They are in good agreement with the reference solutions [10]. With both schemes the contact discontinuities are preserved and do not move with time. Furthermore, the interface computed with the "Order 2 L^2 AP" scheme (when no implicit diffusion is added) is much sharper. However, we see that the L^2 AP scheme presents some spurious oscillations that are reduced when the implicit upwinding is applied (middle).

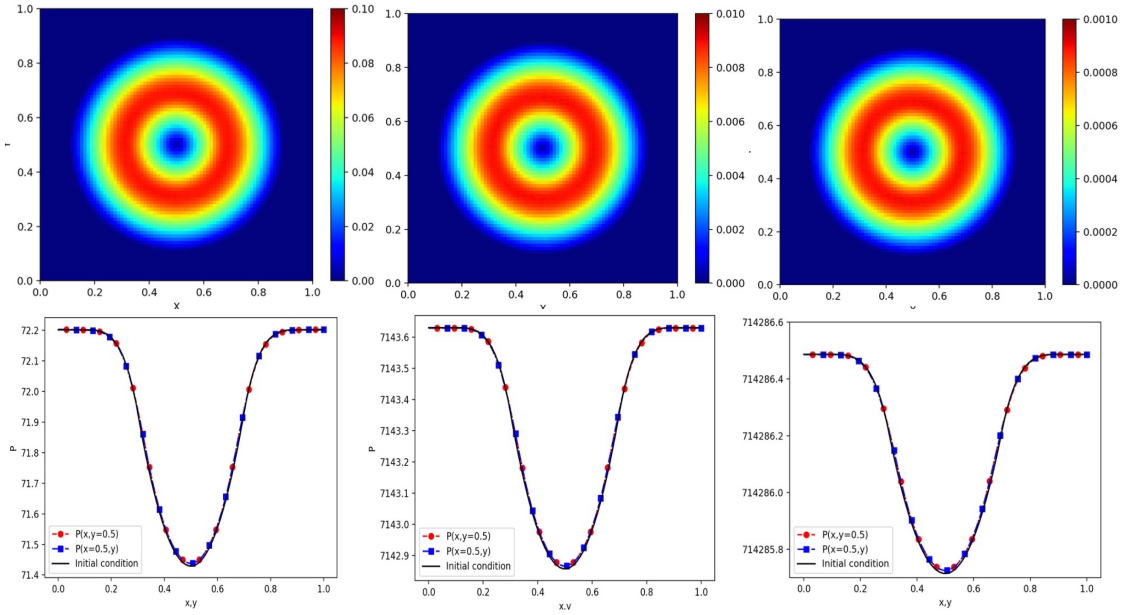

Figure 12: Gresho vortex at time $T = 0.4\,\pi$ given by the "Order 2 L^2 AP" scheme with no minmod limitation for the slopes with 80×80 cells. Top: physical Mach number $|\mathbf{u}|/c$, bottom: pressure profile in the x and y directions for $M = 10^{-1}$ (left), $M = 10^{-2}$ (middle) and $M = 10^{-3}$ (right).

4.7 Double shear layer: Incompressible solution

We consider a test case studied in [5] which consists of a double shear layer in a periodic domain. It is used to validate the asymptotic consistency of our scheme since for small values of ε we can compare our results with a reference solution computed solving the incompressible Euler equations, see [5]. We set $\Omega = [0,1]^2$ and periodic boundary conditions everywhere. The initial data are well prepared to the incompressible regime (divergence free velocity field and constant pressure) and are given by: $\rho(0,x,y) = 1$, $u(0,x,y) = \tanh(30(y-0.25))$ if $y < 0.5$ and $\tanh(30(0.75-y))$ otherwise, $v(0,x,y) = 0.05\sin(2\pi x)$ and $p(0,x,y) = 1$. The shear layer is initially perturbed by a vertical velocity of small amplitude. Then, each of the layers will evolve into large vortices and will be thinned between those rolls. One relevant quantity is the vorticity $w = \partial_x v - \partial_y u$, which we compute using a second order difference approximation.

$$w_{i,j} = \frac{v_{i+1,j} - v_{i-1,j}}{2\,\Delta x} - \frac{u_{i,j+1} - u_{i,j-1}}{2\,\Delta y}.$$

The results are given in Figure 15 in which, we show the contour vorticity plots at time $t = 1.2$ for decreasing values of ε. We observe that for large values of ε the scheme does not capture the incompressible solution while for $\varepsilon = 10^{-3}$ and 10^{-6} the results are in very good agreement with the incompressible solution see [5].

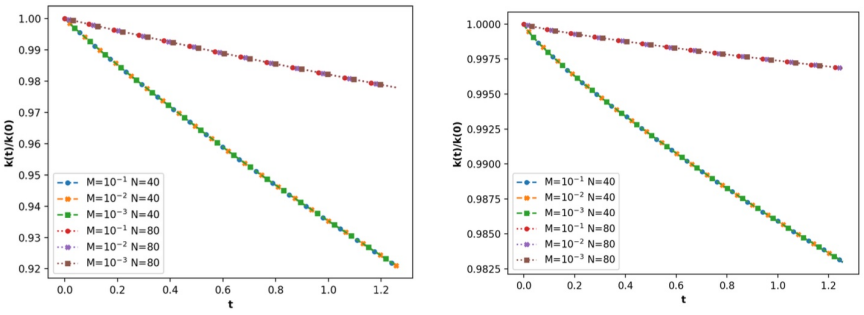

Figure 13: Gresho vortex at time $T = 0.4\,\pi$ given by the "Order 2 L^2 AP" scheme. Kinetic energy for different values of the Mach number $M = 10^{-1}$, $M = 10^{-2}$ and $M = 10^{-3}$. Left: with no minmod limitation, Right: with the minmod limitation .

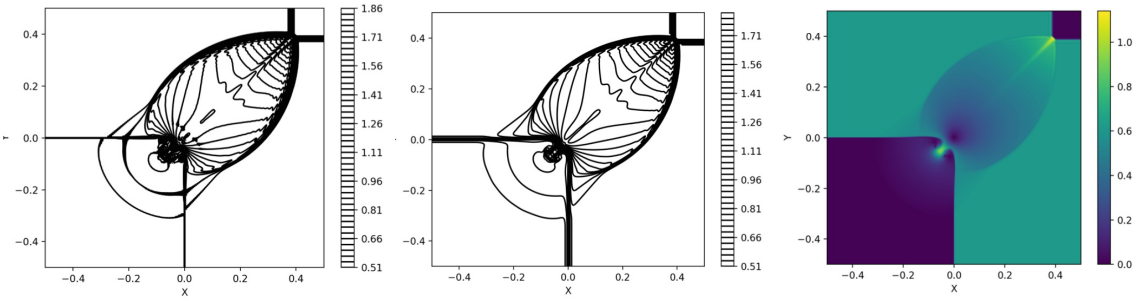

Figure 14: 2D Riemann problem at time $T = 0.25$ with 400×400 cells. Left: Density isolines given by the Order 2 L^2 AP scheme. Middle: Density isolines given by the Order 2 L^∞ AP scheme. Right : Physical Mach number

4.8 Mood procedure

Since we observed that in many situations the full second-order AP scheme can be employed without formation of spurious oscillations and since the TVD AP scheme is only first-order accurate we aim at constructing an optimized AP scheme using the MOOD technique [21], [22] (Multidimensional Optimal Order Detection).
It consists of the following algorithm:

1. We compute the solution with the second-order AP scheme (24)-(25).

2. We apply the detection criteria, then if in a cell j, spurious oscillations are detected then we compute the solution with the TVD AP scheme (28).

We refer to this algorithm as the AP-MOOD scheme for the Euler equations.

The detection of these oscillations is a difficult problem. Many different detection criteria (see for instance [21], [44]) can be found in the literature such as the positivity of the density, a maximum principle on the physical quantities, on the conservative variables... Here, we prefer introduce a new criterion, based on a property verified by the continuous problem. We only consider the

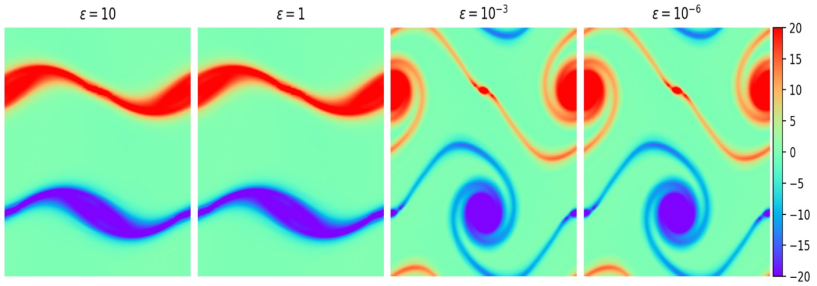

Figure 15: Double shear layer. Vorticity contours given by the "Order 2 L^2 AP" scheme on a 128×128 grid at time t = 1.2 for decreasing values of ε

one-dimensional case, first step for studying the oscillation detection criterion. The extension to multi-dimensional problems is left for future works but for cartesian meshes, the one dimensional criteria can be applied in each directions for the pressure and each component of the velocity.

It is known that at a continuous level and for a Riemann problem at least u or p satisfy the maximum principle. We propose to use this property for detecting spurious oscillations. We introduce a local detection criterion which relies on testing whether both u and p break the maximum principle at the same time. For each cell j, we calculate the following bounds: $(u_{min})_j^n = \min(u_{j-1}^n, u_j^n, u_{j+1}^n)$, $(u_{max})_j^n = \max(u_{j-1}^n, u_j^n, u_{j+1}^n)$, $(p_{min})_j^n = \min(p_{j-1}^n, p_j^n, p_{j+1}^n)$ and $(p_{max})_j^n = \max(p_{j-1}^n, p_j^n, p_{j+1}^n)$. We detect a loss of the maximum principle on u and p simultaneously on a given cell $j \in 1, N_x$ if for $f = p$ and u:

$$f_j^{n+1} < m_{f,j}^n - \text{tol}^n \quad \text{and} \quad f_j^{n+1} > M_{f,j} + \text{tol}^n, \tag{29}$$

where $m_{f,j}^n = \min((f_{min})_j^n, (f_{min})_j^{n-1})$ and $M_{f,j} = \max((f_{max})_j^n, (f_{max})_j^{n-1})$ and where $\text{tol}^n = \mu_{tol} \left(\max_j(f_j^n) - min_j(f_j^n)\right) \max_j(f_j^n) / \min_j(|f_j^n|)$ with μ_{tol} a tolerance parameter which must be chosen so as not to activate the procedure too much in order to be as close as possible to the second-order solution, but so as to activate it enough to significantly reduce the oscillations.

First, we present on Figure 16 the "Several interacting Riemann problems". For this test-case, the oscillations are particularly difficult to detect because some are located in the intermediate values of the variables. We observe that using our local criterion these local oscillations are well captured and corrected by the AP-MOOD procedure on the velocity and pressure profiles. It is interesting to note that in the MOOD procedure, the second-order scheme is replaced only 7 times out of 31 iterations by the TVD-AP scheme. This keeps the results close to the accuracy of the Order 2 AP scheme (see the velocity maximum).

For the second test-case, we consider a shock tube problem with the initial data :

$$\rho(0,x) = 1, \quad u(0,x) = 1, \quad p(0,x) = \begin{cases} 1+\varepsilon & \text{if } x < 0.5, \\ 1 & \text{otherwise.} \end{cases} \tag{30}$$

Periodic boundary conditions are prescribed. In Figure 17 we compare the results given by the four schemes for $\varepsilon = 10^{-2}$ and $\varepsilon = 10^{-4}$. We observe that the Order 1 AP scheme is very diffusive while the Order 2 AP scheme better approximates the solution but presents oscillations increasing as the Mach number decreases. The TVD-AP scheme shows almost no oscillation as the Mach number decreases. In red, we show the results of our AP-MOOD scheme which reduces significantly the

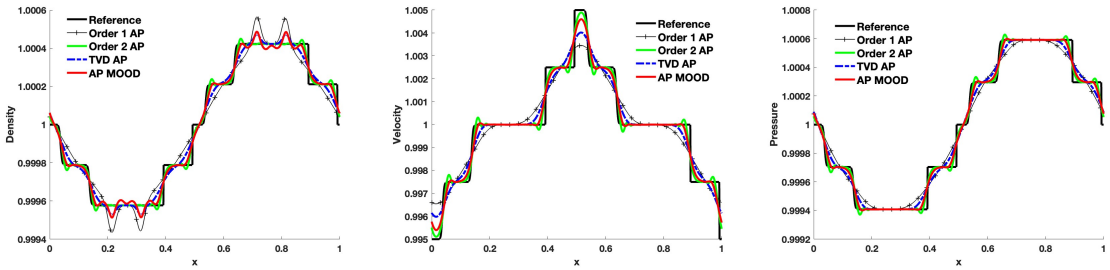

Figure 16: Several interacting Riemann problems (see Section 3.4.2) for $\varepsilon = 10^{-2}$ at $t_{final} = 0.015$ for 1000 cells with $\mu_{tol} = 5 \times 10^{-2}$ in the AP MOOD procedure.

oscillations produced by the Order 2 AP scheme and gives results close to the Order 2 AP scheme. We can see that the tolerance parameter μ_{tol} depends on the test-case but does not depend on ε.

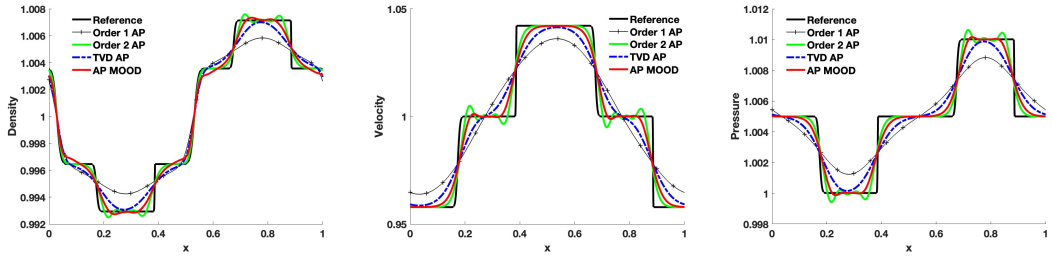

(a) Shock tube problem for $\varepsilon = 10^{-2}$ at $t_{final} = 0.03$ for 500 cells.

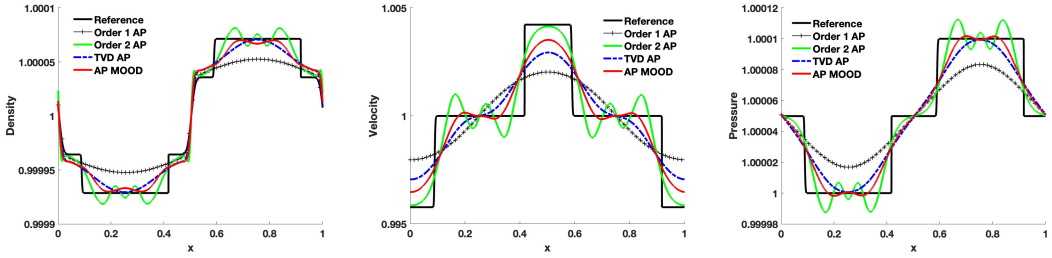

(b) Shock tube problem for $\varepsilon = 10^{-4}$ at $t_{final} = 0.0035$ for 2000 cells.

Figure 17: Shock tube problem (30). Comparison of the Order 1 AP scheme, the second-order AP scheme, the TVD-AP scheme and of the AP-MOOD scheme fixing the tolerance $\mu_{tol} = 1,4 \times 10^{-1}$ (red line) against the reference solution.

5 Conclusion

In this paper we have developed and studied a new linear AP IMEX scheme for the compressible Euler system in the low Mach number limit. We have shown that the chosen flux splitting preserves

the low Mach number limit. We have proved that our resulting AP scheme is asymptotically consistent, it degenerates into a consistent discretization of the incompressible system when the Mach number is sufficiently small. We have performed a Fourier stability analysis showing that our first order scheme is linearly L^2 stable under a CFL condition independent of the Mach number. Furthermore, we have constructed a low-diffusive TVD first-order scheme and using MOOD process, we preserve the low oscillatory properties of the first-order scheme to the second-order scheme. One-dimensional and two-dimensional numerical experiments supported the proposed analysis. In the future, we aim at focusing on local domain decomposition techniques using this AP scheme, the classical scheme for the compressible Euler equations and the classical scheme for the incompressible Euler equations.

References

[1] Commun. Comput Phys T. Alazard, Incompressible limit of the nonisentropic Euler equations with the solid wall boundary conditions. Adv. Differential Equations, 10(1), 19–44, 2005.

[2] K. Asano, On the incompressible limit of the compressible Euler equation. Japan J. Appl. Math. 4, 455–488, 1987.

[3] U. M. Ascher, S. J. Ruuth, R. J. Spiteri, Implicit-explicit Runge-Kutta methods for time-dependent partial differential equations. Appl. Numer. Math. 25(2-3) 151–167, 1997, Special issue on time integration (Amsterdam, 1996).

[4] S. Avgerinos, F. Bernard, A. Iollo, G. Russo, Linearly implicit all Mach number shock capturing schemes for the Euler equations, J. Comp. Phys. 393,278–312, 2019.

[5] J. B. Bell, P. Colella, H. M. Glaz, A second-order projection method for the incompressible Navier-Stokes equations, J. Comp. Phys. 85, 257–283, 1989.

[6] G. Bispen, M. Lukáčová-Medviďová, L. Yelash, Asymptotic preserving IMEX finite volume schemes for low Mach number Euler equations with gravitation, J. Comput. Phys. 335, 222–248, 2017.

[7] S. Boscarino, G. Russo, L. Scandurra, All Mach Number Second Order Semi-Implicit Scheme for the Euler Equations of Gasdynamics, J Sci Comput 77, 850–884 (2018).

[8] W. Boscheri, G. Dimarco, R. Loubère, M. Tavelli, M.-H. Vignal A second order all Mach number IMEX finite volume solver for the three dimensional Euler equations, J. Comp. Phys. 415, 2020.

[9] W. Boscheri, L. Pareschi. High order pressure-based semi-implicit IMEX schemes for the 3D Navier-Stokes equations at all Mach numbers. Journal of Computational Physics, vol. 434, 110206, 2021.

[10] C. W. Schulz-Rinne, J. P. Collins, H. M. Glaz, Numerical Solution of the Riemann Problem for Two-Dimensional Gas Dynamics, SISC, SIAM J. Sci. Comput., vol. 14, (6), 1394-, 1993.

[11] C. Chalons, M. Girardin, S. Kokh, An all-regime Lagrange-Projection like scheme for the gas dynamics equations on unstructured meshes, Communications in Computational Physics (CICP), 20(1), 188–233, 2016.

[12] S. Clain, S. Diot, R. Loubère, A high-order finite volume method for systems of conservation laws—Multi-dimensional Optimal Order Detection (MOOD), J. Comput. Phys. 230(10), 4028–4050, 2011.

[13] F. Cordier, P. Degond, A. Kumbaro, An Asymptotic-Preserving all-speed scheme for the Euler and Navier Stokes equations, J. Comp. Phys. 231, 5685–5704, 2012.

[14] P. Degond, F. Deluzet, A. Sangam, M.-H. Vignal, An Asymptotic Preserving Scheme for the Euler equations in a strong magnetic field, Comp. Phys. 228, 3540–3558, 2009.

[15] P. Degond, M. Tang, All speed scheme for the low Mach number limit of the isentropic Euler equations. Commun. Comput. Phys. 10(1), 1–31, 2011.

[16] P. Degond, S. Jin, J.-G. Liu, Mach-number uniform asymptotic-preserving gauge schemes for compressible flows. Bull. Inst. Math. Acad. Sin. (N.S.) 2 (2007), no. 4, 851-892.

[17] S. Dellacherie, Analysis of Godunov type schemes applied to the compressible Euler system at low Mach number, J. Comp. Phys. 229, 978-1016, 2010.

[18] G. Dimarco, R. Loubère, V. Michel-Dansac, M.-H. Vignal, Second order Implicit-Explicit Total Variation Diminishing schemes for the Euler system in the low Mach regime, J. Comput. Phys., 372, 178–201, 2018

[19] G. Dimarco, R. Loubère, M.-H. Vignal, Study of a new asymptotic preserving scheme for the Euler system in the low Mach number limit, SIAM J. Sci. Comput., 39(5), A2099–A2128, 2017.

[20] G. Dimarco, L. Pareschi, Asymptotic-preserving IMEX Runge-Kutta methods for nonlinear kinetic equations, SIAM J. Num. Anal. 1064–1087, 2013.

[21] S. Diot, S. Clain, R. Loubère, Improved detection criteria for the multi-dimensional optimal order detection (MOOD) on unstructured meshes with very high-order polynomials, Comput. & Fluids, 64, 43–63, 2012.

[22] S. Diot, R. Loubère, and S. Clain, The multidimensional optimal order detection method in the three-dimensional case: very high-order finite volume method for hyperbolic systems, Internat. J. Numer. Methods Fluids, 73(4), 362–392, 2013.

[23] M. Dumbser, V. Casulli, A conservative, weakly nonlinear semi-implicit finite volume scheme for the compressible Navier-Stokes equations with general equation of state, Applied Mathematics and Computation, 2016, vol. 272, issue P2, 479-497

[24] N. Grenier, J.-P. Vila, P. Villedieu, An accurate low-Mach scheme for a compressible two-fluid model applied to free-surface flows, J. Comp. Phys. 252, 1–19, 2013.

[25] S. Gottlieb, C.-W. Shu, E. Tadmor, Strong stability-preserving high-order time discretization methods, SIAM Rev. 43(1), 89–112, 2001.

[26] H. Guillard, A. Murrone, On the behavior of upwind schemes in the low Mach number limit : II. Godunov type schemes, Comp. & Fluids, 33, 655–675, 2004.

[27] H. Guillard, C. Viozat, On the behavior of upwind schemes in the low Mach limit, Comp. & Fluid, 28, 63–86, 1999.

[28] J. Haack, S. Jin, J.G. Liu, An all-speed asymptotic-preserving method for the isentropic Euler and Navier-Stokes equations, Commun. Comput. Phys., 12, 955–980, 2012.

[29] C. Hu and C.W. Shu. Weighted essentially non-oscillatory schemes on triangular meshes, J. Comput. Phys. 150, 97–127, 1999.

[30] S. Klainerman, A. Majda, Singular limits of quasilinear hyperbolic systems with large parameters and the incompressible limit of compressible fluids, Comm. Pure Appl. Math. 34(4), 481–524, 1981.

[31] S. Klainerman, A. Majda, Compressible and incompressible fluids, Comm. Pure Appl. Math. 35(5), 629–651, 1982.

[32] P.-L. Lions, N. Masmoudi, Incompressible limit for a viscous compressible fluid, J. Math. Pures Appl. (9), 77(6), 585–627, 1998.

[33] M. Lukáčová-Medvid'ová, G. Puppo, A. Thomann, An all Mach number finite volume method for isentropic two-phase flow, J. Numer. Math., 31, 175–204, 2023.

[34] G. Métivier, S. Schochet, The incompressible limit of the non-isentropic Euler equations, Arch. Ration. Mech. Anal., 158(1), 61–90, 2001.

[35] G. Métivier, S. Schochet, Averaging theorems for conservative systems and the weakly compressible Euler equations, J. Differential Equations 187, no. 1,106–183, 2003.

[36] V. Michel-Dansac, A. Thomann, On High-Precision $L\infty$-stable IMEX Schemes for Scalar Hyperbolic Multi-scale Equations. Recent Advances in Numerical Methods for Hyperbolic PDE Systems. T. 28. SEMA SIMAI Springer Series. Springer, Cham, 79–94, 2021.

[37] C. D. Munz, M. Dumbser, S. Roller, Linearized acoustic perturbation equations for low Mach number flow with variable density and temperature, J. Comput. Phys., 224, 352–364, 2007.

[38] S. Noelle, G. Bispen, K.R. Arun, M. Lukáčová-Medvid'ová, C. D. Munz, A weakly asymptotic preserving low Mach number scheme for the Euler equations of gas dynamics. SIAM J. Sci. Comput. 36 (2014), no. 6, B989-B1024.

[39] L. Pareschi, G. Russo, Implicit-explicit Runge-Kutta schemes for stiff systems of differential equations, In Recent trends in numerical analysis, volume 3 of Adv. Theory Comput. Math. pages 269–288. Nova Sci. Publ., Huntington, NY, 2001.

[40] S. Schochet, The compressible Euler equations in a bounded domain: existence of solutions and the incompressible limit, Comm. Math. Phys., 104(1), 49–75, 1986.

[41] M. Tang, Second order all speed method for the isentropic Euler equations. Kinet. Relat. Models 5 (2012), no. 1, 155-184.

[42] E. F. Toro, Riemann solvers and numerical methods for fluid dynamics. A practical introduction, Springer-Verlag, Berlin, third edition, 2009.

[43] E.F. Toro, M.E. Vázquez-Cendón, Flux splitting schemes for the Euler equations, Comput. Fluids 70 (2012) 1-12.

[44] F. Vilar, A posteriori correction of high-order discontinuous Galerkin scheme through subcell finite volume formulation and flux reconstruction, J. Comp. Phys., 245, 2019.

[45] J. Zeifang, J. Schütz, K. Kaiser, A. Beck, M. Lukáčová-Medvid'ová, S. Noelle, A Novel Full-Euler Low Mach Number IMEX Splitting, Commun. Comput. Phys., 27, 292, 2020.